Deep-Sea Research Part I 144 (2019) 95–114

Contents lists available at ScienceDirect

Deep-Sea Research Part I

journal homepage: www.elsevier.com/locate/dsri

DOM dynamics in open waters of the Mediterranean Sea: New insights from optical properties

Y. Galletti[a], M. Gonnelli[a], S. Retelletti Brogi[a,b], S. Vestri[a], C. Santinelli[a,*]

[a] Biophysics Institute, Italian National Research Council, Via G. Moruzzi 1, Pisa 56124, Italy
[b] Department of Environment & Energy, Sejong University, Seoul 05006, South Korea

ARTICLE INFO

Keywords:
CDOM
DOC
Carbon cycling
Mediterranean Sea
Fluorescence excitation-emission matrixes
Terrestrial humic-like substances
PARAFAC

ABSTRACT

In the Mediterranean Sea (Med Sea), Dissolved Organic Matter (DOM) dynamics shows some peculiarities that can be investigated by using its optical properties. Despite being a marginal sea, the Med Sea behaves as a miniature ocean for DOM concentrations and distribution. Its surface waters are "greener" than it would normally result from their generally low phytoplankton content and in the deep waters DOC is ~1000 years older and more degraded than in the Atlantic Ocean. These observations suggest a greater contribution of allocthonous substances to the DOM pool in this basin. With this work we aim at presenting new data on optical properties of chromophoric DOM (CDOM) and fluorescent DOM (FDOM) in open sea waters of the Med Sea, in order to investigate the main drivers of CDOM and FDOM dynamics in both surface and deep waters and to get insights into their origin.

Our data confirm the occurrence of DOM with a different composition with respect to the oceans and suggest some differences with respect to other marginal basins, opening intriguing questions about the source and cycle of allocthonous molecules in the open sea waters of the Med Sea. CDOM absorption in the western Med Sea and Ionian Sea is generally lower than that observed in the other marginal seas, but higher than in the oceans. The parallel factor analysis unveiled the presence of one PAH-like and one terrestrial humic-like component that were found in the other marginal basins but that were not found in the open oceans. In contrast to the oceans and most of the marginal seas, only one protein-like component was found. Net production of humic-like FDOM as function of mineralization was not observed in the intermediate and deep waters of the Med Sea, supporting that in this basin CDOM/FDOM dynamics is different than in the oceans. In the surface layer, photobleaching plays a relevant role in the removal of humic-like fluorescence, and the release of both protein-like and humic-like substances occurs in proximity of the deep chlorophyll maximum.

1. Introduction

Dissolved organic matter (DOM) in the oceans contains one of the largest reservoirs of reduced carbon on the Earth, the Dissolved Organic Carbon (DOC) (Hansell et al., 2009). DOC is a key player in the global carbon cycle and in the functioning of marine ecosystems. In the oceans, DOC shows concentrations ranging between 80 μM in surface waters and mid ocean gyres and 34–48 μM in the deep Atlantic and Pacific (Hansell et al., 2009). The DOC pool has been differentiated in various fractions according to their lifetime, going from hours-days (labile, LDOC), to months (semi-labile, SLDOC), years (semi-refractory, SRDOC) up to thousands of years (~16,000 years, refractory, RDOC; ~40,000 years, ultra-refractory, URDOC) (Hansell, 2013). Most of the labile DOC is produced in the ocean epipelagic layer (0–200 m) and this fraction supports the metabolic energy and nutrient demands of heterotrophic prokaryotes (Carlson and Hansell, 2015). A highly variable fraction of DOM is chromophoric (CDOM), it absorbs light at the UV and visible wavelengths and can emit part of the absorbed light as fluorescence (FDOM). CDOM is ubiquitous in marine environments, influences the optical properties of the water column and traces biogeochemical processes and circulation (Nelson and Siegel, 2013). Optical properties (absorption and fluorescence) of CDOM can give information about qualitative changes in DOM pool and its main sources. The parallel factor analysis (PARAFAC) applied to the fluorescence excitation emission matrixes (EEMs) is today one of the most used tools to gain information on CDOM composition and origin (Stedmon et al., 2003; Stedmon and Markager, 2005a, 2005b; Stedmon and Bro, 2008; Jørgensen et al., 2011; Yamashita et al., 2013; Catalá et al., 2015, 2016;

* Corresponding author.
E-mail address: chiara.santinelli@pi.ibf.cnr.it (C. Santinelli).

https://doi.org/10.1016/j.dsr.2019.01.007
Received 4 April 2018; Received in revised form 17 January 2019; Accepted 18 January 2019
Available online 26 January 2019
0967-0637/

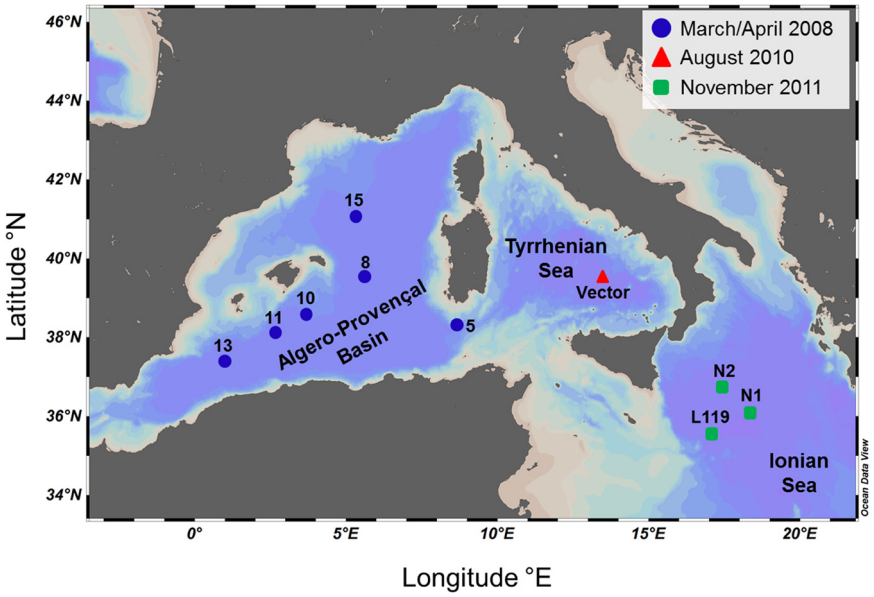

Fig. 1. Study areas and sampling stations.

Gonnelli et al., 2016; Margolin et al., 2018).

DOM dynamics shows some peculiarities in the Mediterranean Sea (Med Sea). Despite being a marginal sea, it shows DOC concentrations and distributions very similar to those observed in the global oceans (Santinelli et al., 2015), but its surface waters (0–20 m) are "greener" than it would normally result from their generally low phytoplankton content (Antoine et al., 2008). This feature can be explained by the unusually high yellow substances content of the surface Med Sea water (Morel et al., 2007), which is about twice that in the Atlantic Ocean at the same latitudes (Morel and Gentili, 2009). The enhanced absorption in the blue and enhanced backscattering in the green parts of the visible spectrum, likely resulting from the presence of submicron Saharan dust in suspension within the upper layer (Claustre et al., 2002), can also explain this observation. In the offshore waters of the western Med Sea (Boussole site) CDOM dominates light absorption at 440 nm (> 50%) all over the year with the exception of March and April, when the absorption is dominated by the photosynthetic pigments of phytoplankton, and it is the only dominant light-absorbing substance below the deep chlorophyll maximum (DCM) (Organelli et al., 2014). In coastal areas, CDOM mainly has a terrestrial origin (Seritti et al., 1998; Vignudelli et al., 2004; Para et al., 2010; Gonnelli et al., 2013; Retelletti Brogi et al., 2015), whereas in the surface offshore waters of the Ligurian Sea, it shows a clear seasonal dynamics related to phytoplankton and microbial activity, suggesting that in the euphotic layer of this area CDOM is mainly autochthonous (Organelli et al., 2014, 2017). A recent extended study about CDOM dynamics showed that in the epipelagic layer community, respiration drives DOC and a_{254} dynamics, whereas water column stability and photobleaching are the main drivers of a_{325} and spectral slope (Catalá et al., 2018). These studies are limited to CDOM absorption, no fluorescence data are reported.

Moving to deep waters (> 1000 m), isotope data unveil that DOC is depleted in both $\Delta^{14}C$ and $\delta^{13}C$ with respect to the deep Atlantic Ocean, suggesting that its pool is ~1000 years older than in the Atlantic Ocean (Santinelli et al., 2015). This finding was explained by the replacement of 10% and up to 45% of the Atlantic RDOC entering the basin by allocthonous (isotopically lighter and older) DOC (Santinelli et al., 2015). The different chemical composition of DOC in the Med Sea with respect to the oceans is also supported by the Fourier Transform Ion Cyclotron Resonance mass spectroscopy (FT-ICR-MS) data (Martínez-Pérez et al., 2017a). These authors showed that DOC in the Med Sea outflow is more degraded than in the Atlantic inflow. Few information is reported about CDOM and/or FDOM dynamics in intermediate and deep waters (Bracchini et al., 2010; Martínez-Pérez et al., 2017a, 2017b; Catalá et al., 2018) to support these observations and only one paper reports basin-wide patterns of absorption coefficients and spectral slopes, showing that below the euphotic zone, CDOM dynamics is mainly shaped by water masses mixing and basin-scale mineralization (Catalá et al., 2018).

Despite CDOM is a relevant player in the biogeochemistry and bio-optical properties of the Med Sea, many aspects need to be clarified in particular about CDOM and FDOM dynamics in open sea waters. With this work we aim at presenting new data on DOC and optical properties (both absorption and fluorescence) of CDOM in open sea waters of the Med Sea, in order to: (i) investigate the main drivers of CDOM and FDOM dynamics in both surface and deep waters of the Med Sea; (ii) get insights into CDOM and FDOM origin in the offshore waters of the Med Sea. These data will also contribute to test the hypothesis that in the Med Sea DOM pool is constituted by a larger fraction of allocthonous (humic-like, yellow substances) material than in the oceans, despite the DOC concentration and distribution is exactly the same as in the open ocean.

2. Materials and methods

2.1. Study sites and sample collection

Samples for DOC, CDOM and FDOM analysis were collected in open sea waters of the Med Sea during 3 oceanographic cruises carried out in March/April 2008, August 2010 and November 2011 on board the R/V *Urania* of the Italian National Research Council (CNR) (Fig. 1 and Table 1).

At all stations pressure, salinity, temperature and oxygen were measured through a SBE 911 plus CTD, equipped with a rosette sampler with 24 × 10-L Niskin bottles. The CTD-rosette system was lowered at a speed of 1 m s^{-1}. The data were processed in real time, viewed and corrected to eliminate errors. CTD-oxygen was calibrated by Winkler titration (Williams and Jenkinson, 1982) of selected discrete samples. Oxygen saturation was calculated using calibrated CTD data and the solubility equations of Garcia and Gordon (1992) and coefficients of Benson and Krause (1984). Apparent Oxygen Utilization (AOU) was calculated as difference between oxygen saturation and oxygen at a given depth.

Chlorophyll-a fluorescence (Chl-a) was measured using a SEA-TECH fluorimeter mounted on the rosette sampler. Data are reported as

Table 1
Details of the sampling stations. $Index_{str}$ is the stratification index, MLD is the Mixed Layer Depth.

Study area	Cruise	Date	Time h	Station	Lat °N	Long °E	$Index_{str}$ kg m^{-3}	MLD m
Algero-Provençal Basin	Sesame S-IT4	03-29-2008	13:13	5	38.32	08.65	0.56	> 250
		03-30-2008	10:46	8	39.50	05.65	0.93	29 (139)
		04-02-2008	14:01	10	38.62	03.65	1.12	70
		04-02-2008	7:50	11	38.18	02.65	1.23	38 (86)
		04-01-2008	12:26	13	37.43	01.00	1.27	38
		04-05-2008	11:31	15	41.03	05.33	0.30	56
Tyrrhenian Sea	Venus-1	08-18-2010	2:13	Vector	39.30	13.30	3.86	19
Ionian Sea	SICSIA 2011	11-26-2011	19:51	N1	36.14	18.33	1.39	57
		11-27-2011	2:49	N2	36.74	17.43	1.22	58
		11-25-2011	7:48	L119	35.61	17.08	1.88	39

Fluorescence Units (Fl.U.). Assuming that no drift in the instrument response occurred within each cruise, fluorescence profiles are used to highlight differences in autotrophic biomass among stations and to determine the depth interval of the DCM (Santinelli et al., 2008).

The index of stratification ($Index_{str}$) was calculated as the difference between density at 5 m and at 200 m, according to Santinelli et al. (2013).

Mixed layer depths (MLD) were estimated from CTD temperature profiles, and defined by a ≥ 0.1 °C deviation with respect to the temperature at 5 m depth, in agreement with Pérez et al. (2016).

2.2. Sample treatment

Samples for DOC, CDOM and FDOM measurements were collected along the water column at the following depths: 2, 20, 50, 75, 100, 150, 200, 400, 500, and every 250 m until the bottom. Samples were collected in 200 mL dark glass bottles, preconditioned with filtered deep seawater and rinsed 3 times with the sample before its collection. Samples were immediately filtered on board via sterile 0.2 µm nylon filters (Sartorius, 17845-ACK) under pressure of high-purity air (Santinelli et al., 2010). Filtered samples were stored at 4 °C in the dark until the analysis, carried out within 1 month from the sampling. No change in DOC concentration and optical properties of CDOM was observed within this period (Santinelli et al., 2010).

2.3. DOC analysis

DOC measurements were carried out with a Shimadzu TOC-VCSN, by high-temperature catalytic oxidation. Samples were acidified with HCl 2 N and sparged for 3 min with CO_2-free pure air in order to remove inorganic carbon. From 3–5 replicate injections were performed until the analytical precision was lower than 1% (± 1 µM). A 5-point calibration curve was done by injecting standard solutions of potassium hydrogen phthalate between 20 and 130 µM. At the beginning and at the end of each analytical day, the system blank was measured using Milli-Q water and the functioning of the instrument was checked by comparison of data with DOC Consensus Reference Material (CRM) (Hansell, 2005) (batch#7-2007, batch#10-2010/Lot#5-10, batch#11-2011/Lot#03-11, Consensus values: 41–44 µM, measured concentration: 41.9 ± 1.3 µM, standard error = 0.23 µM, n = 39). For further analytical details see Santinelli et al. (2010).

2.4. CDOM optical properties

2.4.1. Absorption measurements

CDOM absorbance was measured throughout the UV and visible spectral domains (230–700 nm) with a resolution of 0.5 nm, by using a JASCO Spectrophotometer V-550 and a 10 cm quartz cuvette. The photometric reproducibility of the instrument is ± 0.001 Abs. The spectrum of Milli-Q water, measured in the same conditions, was subtracted from each sample. Initial, intermediate and final blanks were measured to check for the instrument functioning. The absorbance (A) was converted into absorption coefficients (a) by using Eq. (1):

$$a_\lambda = 2.303 \bullet \frac{A_\lambda}{L} + k \quad (1)$$

where A_λ is the absorbance at the wavelength λ and L is the cuvette pathlength expressed in m and k is an offset calculated as the mean absorbance between wavelengths 650 nm and 700 nm (approximately zero) (Green and Blough, 1994). The absorption coefficient (a_λ) was calculated at different wavelengths (254, 280, 325 nm), in order to facilitate the comparison with data reported in the literature. a_{254} is considered representative of the CDOM pool, since it is a proxy for the abundance of conjugated carbon double bounds (Lacowicz, 2006), it is therefore used to gain quantitative information on the whole CDOM pool.

The CDOM absorption spectrum is typically described using Eq. (2), according with Bricaud et al. (1981):

$$a_\lambda = a_{\lambda_0} \bullet e^{-S(\lambda-\lambda_0)} \quad (2)$$

where S is the spectral slope coefficient in the λ-λ_0 nm spectral range. S was estimated over the 275–295 nm spectral range ($S_{275–295}$), because this range is characterized by the greatest variations and it has been demonstrated to be a reliable proxy of CDOM average molecular weight (Helms et al., 2008) and a potential indicator of photobleaching and DOM source in marine environment (Helms et al., 2008; Fichot and Benner, 2012).

The specific ultraviolet absorbance at 254 nm ($SUVA_{254}$) was calculated by dividing the a_{254} by DOC concentration in units mg C L^{-1} (Weishaar et al., 2003). $SUVA_{254}$ has been reported to be strongly correlated with percent aromaticity, it is therefore considered a useful parameter for estimating the dissolved aromatic carbon content in aquatic systems (Weishaar et al., 2003).

Five measurements (including all handling steps) were carried out on the same seawater sample within the period of the analysis and they showed that the reproducibility of measurements was approximately ± 0.01 m^{-1} for a_{254} and a_{280}, ± 0.003 m^{-1} for a_{325} and ± $4 \cdot 10^{-4}$ nm^{-1} for $S_{275–295}$, that is ~1% for all the parameters.

2.4.2. Fluorescence Excitation Emission Matrixes (EEMs)

Fluorescence Excitation Emission Matrixes (EEMs) were recorded by using the Fluoromax4 spectrofluorometer (model FP770 Horiba) with a 1 × 1 cm quartz cuvette in the range 250–450 nm for the excitation and 300–600 nm for the emission. The EEMs were corrected for instrumental bias and subtracted by the EEM of Milli-Q water measured in the same conditions (blank). The Rayleigh and Raman scatter peaks were removed by using the monotone cubic interpolation (shape-preserving) (Carlson and Fritsch, 1989), since water subtraction did not completely

remove their signals (Gonnelli et al., 2016; Margolin et al., 2018). EEMs were normalized to the water Raman signal, dividing the fluorescence by the integrated Raman band of Milli-Q water (λ_{ex} = 350 nm, λ_{em} = 371–428 nm), measured the same day of the analysis (Lawaetz and Stedmon, 2009). The fluorescence intensity is therefore reported as equivalent water Raman Units (R.U.). This standardized method was chosen because it is rapid, simple and suitable for routine measurements. No significant variation was observed in the integral of the Raman peak from repeated measurements during the period of the analysis (< 2%). In order to check the repeatability of our measurements the same sample was analyzed 5 times during a period of 3 months, the results showed that the variation was less than 2% for all the components.

The 103 EEMs were elaborated with the parallel factor analysis (PARAFAC) by using the DOMFluor toolbox (Stedmon and Bro, 2008). The validation of the model was done by visual inspection of the residuals, split half analysis and percentage of explained variance (99.5%). PARAFAC components were compared with the spectra of commercial compounds: Suwannee River (Suwriver) fulvic acids (FA) and Pahokee Peat humic acids (HA) from the International Humic Substances Society (IHSS) and tryptophan (Trp) from Sigma–Aldrich. Solutions of each individual compound were prepared by dissolving them in deep-sea water, with a low fluorescent signal, to a final concentration of: 0.5 mg mL^{-1} for HA and FA, and 1 μg mL^{-1} for Trp. Single fluorescence emission spectrum of these solutions was measured with the Fluoromax4, with 1 × 1 cm quartz cuvette. The spectrum of the deep-sea water, used for the dilution, was subtracted from each spectrum.

2.5. Statistics

Differences were tested by using one-way ANOVA and the Tukey test and were considered significant when $p < 0.05$ (Origin 8.5.1 software).

The correlations were investigated by using Origin 8.5.1 software and were considered robust when $p < 0.0001$ for the whole dataset and $p < 0.05$ for the single areas.

3. Results

3.1. PARAFAC components

The PARAFAC analysis, applied to the 103 EEMs measured in this study, allowed for the identification of 5 groups of fluorophores (components) in the FDOM pool. In order to identify these components, their spectra were compared to (i) spectra of commercial Trp, HA and FA dissolved in seawater, (dotted lines in Fig. 2), (ii) similar components reported in the literature and (iii) matching spectra obtained from the OpenFluor database (plugin for OpenChrom, version 1.3.0; Murphy et al., 2014). These spectra were considered similar when the Tucker's congruence coefficient (TCC) exceed 0.95 (Table 2).

Component 1 ($C1_{PAH}$) shows spectral characteristics similar to those of anthracene (Ex/Em: 245/382 nm) and pyrene (Ex/Em: 240–270/374–392 nm) dissolved in water (Ferretto et al., 2014) (Fig. 2). The excitation maximum at 250 nm implies low conjugation degree and low molecular weight material, typical of phenols and/or quinones of terrestrial origin. A similar component was found in the China and Okhotsk Seas, in ballast waters and in harbors (Table 2). $C1_{PAH}$ can be therefore attributed to PAH contaminants and it was identified as a terrestrial component with an anthropic origin.

Components 2 ($C2_{t\text{-}hum}$) and 3 ($C3_{t\text{-}hum}$) show spectral characteristics typical of terrestrial humic-like compounds (Fig. 2; Table 2). The emission spectrum of $C2_{t\text{-}hum}$ is very similar to that of Suwannee River FA. The Suwannee River rises in the Okefenokee Swamp in south Georgia and the decomposing vegetation is the main source of DOC to its waters (Malcolm et al., 1982). In the literature, $C2_{t\text{-}hum}$ was attributed to humic-like fluorophores derived by terrestrial input exported from natural or agricultural catchments (Stedmon and Markager, 2005a). Fluorescence spectra similar to those of $C2_{t\text{-}hum}$ were found to correlate with lignin (Walker et al., 2009), a biomarker of terrestrial plant material, further supporting its terrestrial origin. $C2_{t\text{-}hum}$ matched with 21 models in the OpenFluor, of which only 2 relative to samples collected in offshore and deep ocean waters (Yamashita et al., 2010b; Jørgensen et al., 2011) (Table 2).

The emission spectrum of $C3_{t\text{-}hum}$ overlaps the emission spectrum of the Pahokee peat humic acids (Fig. 2), that is a typical agricultural peat soil of the Florida Everglades, formed in organic deposits of freshwater marshes. A similar component was found in estuaries and marginal sea (Baltic and North Sea, Black Sea and South Atlantic Bight) (Table 2). No similar component was found in offshore and deep ocean waters.

Component 4 ($C4_{m\text{-}hum}$) shows spectral characteristics similar to those of marine humic-like substances (peak M; Coble, 1996), and is attributed to humic-like substances produced in-situ by phytoplankton and microbial activity (Stedmon and Markager, 2005b; Murphy et al., 2006, 2008; Zhao et al., 2017). However, the small shoulders at 250 nm and 310 nm could imply that the there is an overlap with C1 and that the two components were not very well resolved by PARAFAC.

Component 5 ($C5_{Trp}$) shows features typical of tryptophan-like fluorescence as supported by the very good overlapping with the spectra of commercial Trp (Fig. 2). A similar component was observed in both open ocean waters and in marginal seas (Table 2).

Taking into consideration all the samples collected along the water column in the 3 areas, $C1_{PAH}$ shows a robust linear correlation with $C2_{t\text{-}hum}$. The correlation improves when only the samples collected in the upper 200 m of the water column are taken into consideration, whereas it is weaker in the intermediate and deep waters (200 m to the bottom) (Table 3). $C2_{t\text{-}hum}$ shows a good linear correlation with both $C3_{t\text{-}hum}$ and $C4_{m\text{-}hum}$, that strongly improves for $C3_{t\text{-}hum}$ in the upper 200 m. $C3_{t\text{-}hum}$ and $C4_{m\text{-}hum}$ show a good linear correlation in the upper 200 m, that is completely lost below 200 m. Finally, $C4_{m\text{-}hum}$ and $C5_{Trp}$ shows a good linear correlation in the intermediate and deep waters that is lost in the upper 200 m.

3.2. Physical characteristics of the study area

In order to simplify the representation of the results, the stations were assembled in 3 groups based on their thermohaline properties (Fig. S1), that correspond to the 3 sampled areas: APB = Algero-Provençal Basin, TS = Tyrrhenian Sea and IS = Ionian Sea. Intermediate and deep waters at station 5, located in the Sardinian Channel (Fig. 1), show thermohaline properties more similar to those at the Vector station than at the other stations sampled in the APB (Fig. S1); this station was therefore included in the TS group. The vertical profiles of mean DOC, AOU, CDOM and FDOM components were calculated taking into consideration the 3 groups of stations.

3.3. Vertical profiles of DOC and AOU

DOC showed the highest and most variable concentrations (50–84 μM) in the surface layer (0–100 m) (Fig. 3). Average values in the upper 100 m were significantly lower ($p < 0.05$) in the APB (57 ± 4 μM) than in the IS and TS (64 ± 5 μM). In the intermediate layer, DOC gradually decreased with depth (Fig. 3) to reach the lowest average concentration (40 ± 1 μM in the WM, 42 ± 3 μM in the TS and 39 ± 2 μM in the IS) between 750 and 2000 m. Below 2000 m, the mean values were almost constant (42–43 μM) in the 3 areas, with a slight increase in the samples close to the bottom, in particular in the APB (40–49 μM, 2500-bottom). Vertical profiles of AOU were opposite to those of DOC. The lowest values were observed in the surface layer, followed by a maximum between 200 and 500 m in the APB and TS (81 ± 3 and 73 ± 2 μM, respectively), and in correspondence with the DOC minimum (1000–1500 m) in the IS (66 ± 4 μM). In the deep

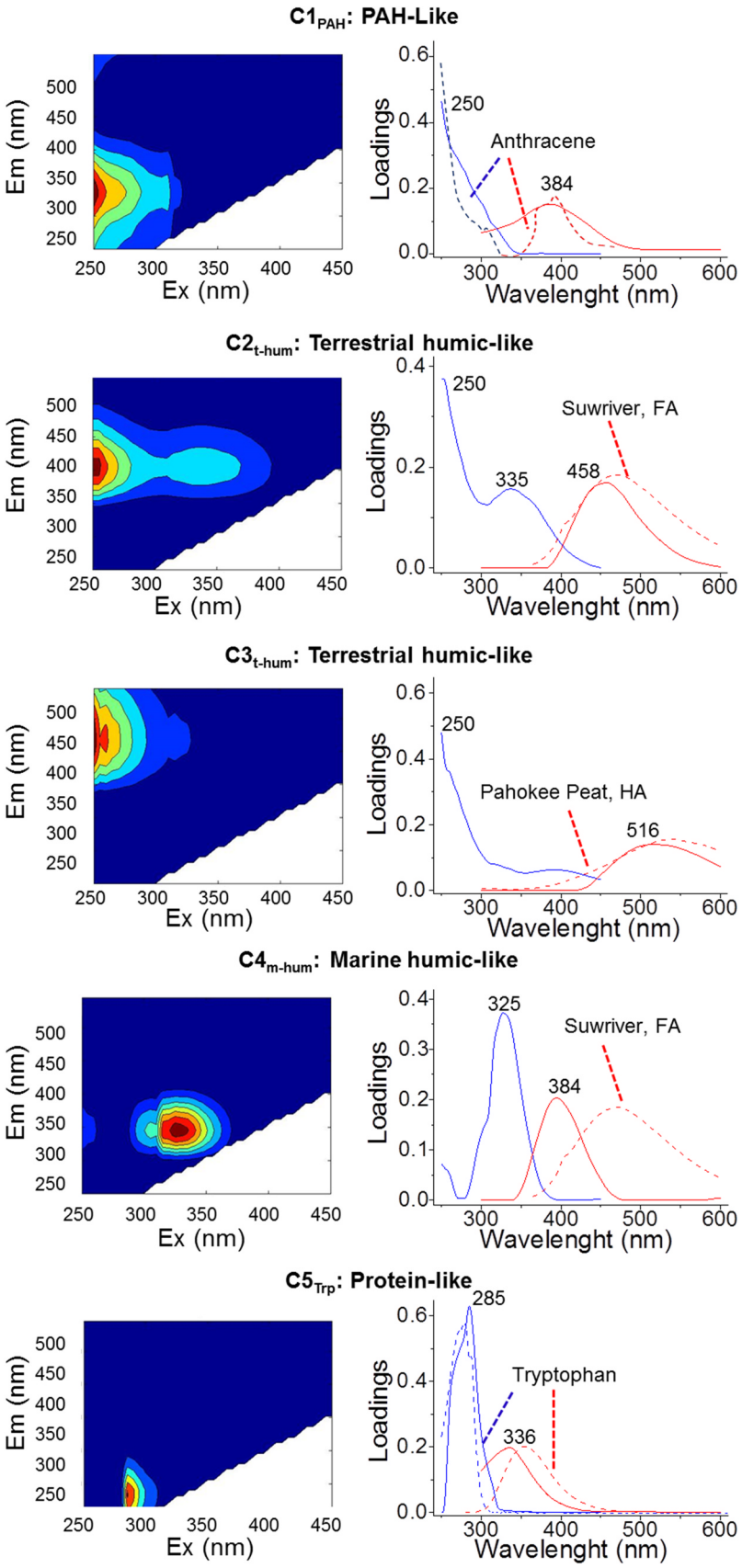

Fig. 2. Fluorescence characteristics of the five components, dataset = 103 EEMs. In the graphs on the right, excitation (blue) and emission (red) spectra of the five components are shown. The spectra are overlapped to those of commercial substances (dotted lines). (For interpretation of the references to color in this figure legend, the reader is referred to the web version of this article.)

Table 2
Identification of the 5 components through the comparison with literature data. Tucker's congruence coefficient (TCC) is reported for matching spectra obtained from the OpenFluor database. In bold are indicated components referring to the marginal seas.

Component	Ex/Em	Identification	Similar to	TCC	
1 $C1_{PAH}$	250(310)/384	*PAH-like of terrestrial origin*	Pacific and Atlantic (C4)	NA	Murphy et al. (2008)
			China Sea (C2)	NA	Wang et al. (2017)
			Okhotsk Sea (C1)	NA	Granskog et al. (2015)
			Ballast water (C4)	NA	Murphy et al. (2006)
2 $C2_{t\text{-}hum}$	250(335)/458	*Terrestrial humic-like substances (Fulvic Acids)*	Peaks "A" and "C"	NA	Coble (1996)
			Epipelagic oceans (C1)	NA	Catalá et al. (2016)
			Dark oceans (C1)	NA	Catalá et al. (2015)
			Black Sea (C2)	NA	Margolin et al. (2018)
			China Sea (C1)	NA	Wang et al. (2017)
			China Sea (C1)	NA	Zhu et al. (2018)
			Okhotsk Sea (C2)	NA	Granskog et al. (2015)
			Aegean Sea (C1)	NA	Pitta et al. (2017)
			Horsens Estuary, Denmark (C4)	NA	Stedmon and Markager (2005a)
			Florida Keys (C2)	NA	Yamashita et al. (2013)
			Ballast water (C8)	NA	Murphy et al. (2006)
			Wetland (C1)	0.987	Yamashita et al. (2010a)
			Patagonia lakes (C2)	0.985	Cárdenas et al. (2017)
			Baltic Sea (C1)	0.984	Stedmon et al. (2007)
			Wastewater (C2)	0.981	Murphy et al. (2011)
			Wastewater (C1)	0.978	Murphy et al. (2011)
			South Atlantic Bight (C1)	0.972	Kowalczuk et al. (2009)
			Ocean off-shore (C1)	0.970	Jørgensen et al. (2011)
			Ocean off-shore (C1)	0.955	Yamashita et al. (2010b)
3 $C3_{t\text{-}hum}$	250(395)/516	*Terrestrial humic-like substances (Humic Acids)*	Peaks "A" and "C"	NA	Coble (1996)
			Ballast water (C3)	NA	Murphy et al. (2006)
			South Atlantic Bight (C4)	NA	Kowalczuk et al. (2009)
			Florida Keys (C4)	0.959	Yamashita et al. (2013)
			Baltic Sea (C3)	NA	Stedmon et al. (2007)
			Horsens Estuary, Denmark (C2)	NA	Stedmon and Markager (2005a)
			Shark Bay Estuary (C2)	0.958	Cawley et al. (2012)
			Baltic and North Sea (C2)	0.952	Osburn and Stedmon (2011)
			Black Sea (C4)	NA	Margolin et al. (2018)
4 $C4_{m\text{-}hum}$	325/394	*Marine humic-like substances*	Marine humic peak "M"	NA	Coble (1996)
			Aegean Sea (C2)	NA	Pitta et al. (2017)
			Baltic Sea (C2)	NA	Stedmon et al. (2007)
			Ocean off-shore (C4)	NA	Jørgensen et al. (2011)
			Epipelagic oceans (C2)	NA	Catalá et al. (2016)
			Dark oceans (C2)	NA	Catalá et al. (2015)
			Ballast water (C2)	NA	Murphy et al. (2006)
			Horsens Estuary, Denmark (C5)	NA	Stedmon and Markager (2005a)
			South Atlantic Bight (C3)	NA	Kowalczuk et al. (2009)
			Florida Keys (C1)	NA	Yamashita et al. (2013)
5 $C5_{Trp}$	285/336	*Protein-like (Tryptophan)*	Peak "T"	NA	Coble (1996)
			Horsens Estuary, Denmark (C7)	NA	Stedmon and Markager (2005a)
			Baltic Sea (C5)		Stedmon et al. (2007)
			Ballast water (C6)	NA	Murphy et al. (2006)
			Ocean off-shore (C5)	NA	Jørgensen et al. (2011)
			Florida Keys (C5)	NA	Yamashita et al. (2013)
			Mesocosm, Baltic Sea (C6)	NA	Stedmon and Markager (2005b)
			South Atlantic Bight (C6)	NA	Kowalczuk et al. (2009)
			Aegean Sea (C4)	NA	Pitta et al. (2017)
			Baltic and North Sea (C6)	NA	Osburn and Stedmon (2011)
			Epipelagic oceans (C3)	NA	Catalá et al. (2016)
			Dark oceans (C3)	NA	Catalá et al. (2015)
			Black Sea (C5)	NA	Margolin et al. (2018)
			China Sea (C4)	NA	Wang et al. (2017)
			China Sea (C3)	NA	Zhu et al. (2018)
			Okhotsk Sea (C3)	NA	Granskog et al. (2015)

waters, AOU was almost constant with depth in the TS (69–72 μM, 2500-bottom), while in the APB and IS it slightly decreased below 500–1000 m, in correspondence with the DOC increase (Fig. 3).

3.4. Vertical profiles of CDOM

Taking into consideration all the data collected in this study, a_{254}, a_{280}, and a_{325} ranged between 0.69 and 1.54 m^{-1}, 0.07–0.33 m^{-1}, 0.09–0.28 m^{-1}, respectively. $S_{275–295}$ ranged between 0.02 and 0.04 nm^{-1} with the highest values in the surface layer of the TS and IS. The lowest values of a_{254} were observed between 750 and 2000 m in the IS (0.36 ± 0.02 m^{-1}), in correspondence with $S_{275–295}$ values of 0.030 nm^{-1}.

The vertical profiles of mean a_{254} showed the highest values in the surface layer (0–100 m) (0.8 ± 0.09 m^{-1}), a sharp decrease below the pycnocline and values almost constant (0.36–0.49 m^{-1}) between 500 and 1000 m and the bottom (Fig. 3). Vertical profiles of a_{254} were very similar to those of DOC, with a highly significant correlation between the 2 variables (DOC = 15(± 2) + 32(± 1)·a_{254}; r^2 = 0.80, $p < 0.0001$; n = 119) (Fig. 4, Table 5). The linear correlation between DOC and a_{254} is maintained, even if it is less robust, when only the samples collected in the upper 200 m are taken into consideration (DOC

Table 3
Values of r^2 and p for the linear correlations among the 5 components, taking into consideration all the data collected in this study. All the correlations are direct. Negative correlations are indicated in italic.

	$C1_{PAH}$			$C2_{t\text{-}hum}$			$C3_{t\text{-}hum}$			$C4_{m\text{-}hum}$		
	0-btm	0–200	200-btm	0-btm	0–200	200-btm	0-btm	0–200	200-btm	0-btm	0–200	200-btm
$C1_{PAH}$												
$C2_{t\text{-}hum}$	**0.50****	**0.58****	0.35**									
$C3_{t\text{-}hum}$	0.21**	0.40**	0.11*	**0.57****	**0.75****	0.36**						
$C4_{m\text{-}hum}$	0.29**	0.25**	0.40**	**0.56****	**0.56****	**0.56****	0.33**	**0.51****	0.11*			
$C5_{Trp}$	0.36**	0.20*	**0.53****	0.11*	0.03	0.27**	0.01	*0.01*	0.04	0.08*	*0.01*	**0.53****

btm = Bottom. Values of $r^2 > 0.5$ are in bold.
* $p < 0.005$.
** $p < 0.0001$.

$= 22(\pm 6) + 27(\pm 5)\cdot a_{254}$; $r^2 = 0.40$, $p < 0.0001$; $n = 51$), whereas the correlation is completely lost when the data collected in the upper 200 m are excluded.

3.5. Vertical profiles of FDOM

The average vertical profiles of $C1_{PAH}$ and the 3 humic-like components ($C2_{t\text{-}hum}$, $C3_{t\text{-}hum}$ and $C4_{m\text{-}hum}$) were similar in the 3 areas, with the lowest intensities in the surface layer and an increase to reach a subsurface maximum, well visible in the TS and IS (Fig. 5). Below 150 m, a decrease was observed with intermediate and constant fluorescence values until the bottom. Along the water column, $C2_{t\text{-}hum}$ and $C3_{t\text{-}hum}$ fluorescence was significantly higher ($p < 0.05$) in the APB than in the IS and TS. No significant difference was observed for $C4_{m\text{-}hum}$.

The average vertical profiles of the protein-like fluorescence ($C5_{Trp}$) showed the highest intensity in the surface layer (0–20 m) and a gradual decrease with depth in the 3 areas to reach values 2-fold lower

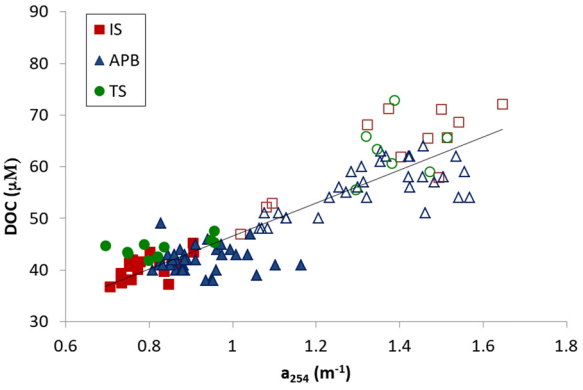

Fig. 4. Correlation between DOC and a_{254} taking into consideration all samples. Empty symbols refer to samples collected in the upper 200 m, filled symbols to samples collected between 200 m and the bottom.

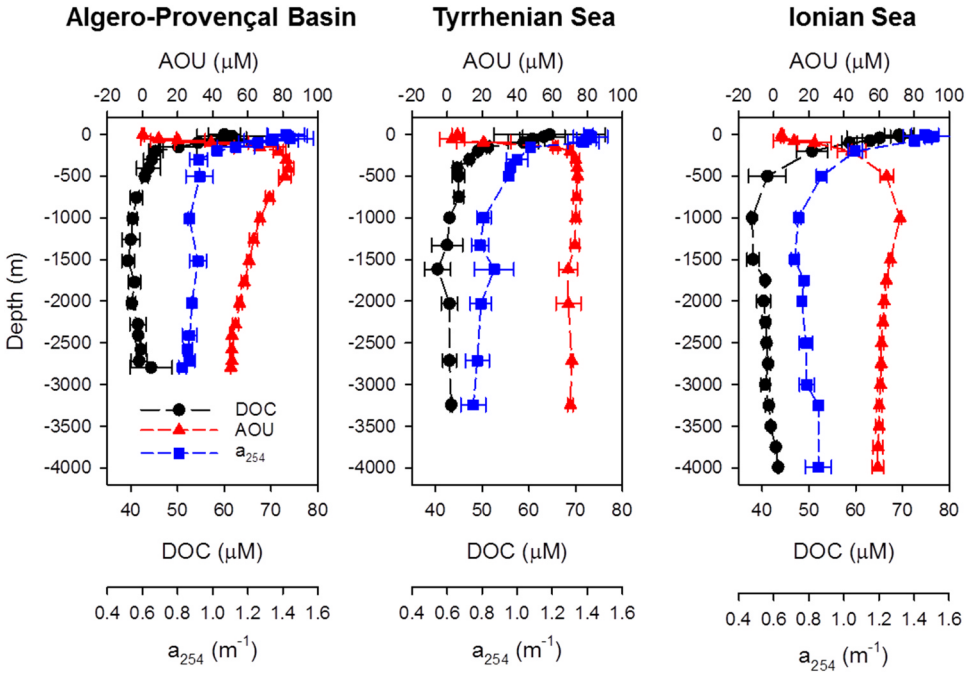

Fig. 3. Vertical profiles of mean DOC, AOU and CDOM (a_{254}) for the 3 areas. Error bars refer to the standard deviation among stations.

Table 4
Comparison of salinity, DOC concentrations and CDOM data among the Med Sea, the other marginal seas and the oceans.

Basin	Salinity	DOC (μM)	CDOM (m^{-1})	$SUVA_{254}$ ($m^2\ g^{-1}C$)	$S_{275–295}$ (nm^{-1})	Reference
Med Sea	37–39*	37–84*	0.07–0.33 (a_{325})*	0.6–1.1*	0.020–0.035*	*This study
			0.69–1.65 (a_{254})*			
			0.32–0.92 (a_{280})*			
			0.05–3.22 (a_{355})*		0.025–0.045[a]	
	36.5–39.5[a]	35–75[a]	0.5–1.3 (a_{254})[a]		0.025–0.045[a]	[a]Catalá et al. (2018)
			0.05–0.27 (a_{325})[a]		**S_R = 1.75–3.25**[a]	
Baltic Sea	6.8 ± 0.1[b]	708 ± 58[b]	3.0–5.8 (a_{350})[c]	2[b]	0.025[b]	[b]Rowe et al., (2018)
	10–20[d]					[c]Stedmon et al. (2007)
		300[d]	4–5 (a_{300})[d]			[d]Osburn and Stedmon (2011)
North Sea	20–35[d]	62–185	1–3 (a_{300})[d]	0.55–4.42[e]	0.021 ± 0.007[e]	[e]Painter et al. (2018)
		(109 ± 16)[e]				
	32–35.5[e]	100–250[d]	0.09–2.74 (a_{375})[e]		**S_R = 1.5–12.9**[e]	
Black Sea	18–22.3[f]	113–205[f]	3.58–8.66 (a_{254})[g]	0.9–2.61[g]	0.026–0.034[g]	[f]Margolin et al. (2016)
			0.46–1.31 (a_{325})[g]			[g]Margolin et al. (2018)
South China Sea	26–35[h,i]	57–117[l]	1.1–1.5 (a_{280})[h]		0.027–0.031[h]	[h]Lin et al. (2012)
			0.26–4.57 (a_{280})[i]		0.031 ± 0.009[i]	[i]Zhou et al. (2018)
			0.07 to 0.20 (a_{350})[m]		0.02–0.05[m]	[l]Meng et al., (2017)
						[m]Wang et al. (2017)
Okhotsk Sea	15–34[n]	60–400[n]	0.24–0.31 (a_{350})[o]			[n]Nakatsuka et al., (2004)
						[o]Granskog et al. (2015)
Oceans	34–37[s]	34–80[s]	0.05–0.25 (a_{325})[p]		0.04–0.05[q]	[p]Nelson et al. (2010)
			0.05–0.50 (a_{325})[q]			[q]Catalá et al. (2015)
			0.04–0.25 (a_{325})[r]			[r]Nelson, Gauglitz (2016)
						[s]Hansell et al. (2009)

below 1000 m than in the surface waters ($p < 0.05$) (Fig. 5). A peak around 2000 m was observed in the 3 areas. $C5_{Trp}$ fluorescence in the upper 200 m was 1.6-fold higher ($p < 0.05$) in the APB than in the IS and TS.

3.6. Surface layer

Due to the high variability of the surface layer and to the different period of the cruises (Table 1), a zoom (0–250 m) of the vertical profiles of chlorophyll, temperature, density, salinity, DOC, a_{254}, $S_{275–295}$, $C3_{t\text{-}hum}$, $C4_{m\text{-}hum}$ and $C5_{Trp}$ is reported for each station separately (Figs. 6, 7 and 8). $C3_{t\text{-}hum}$ is reported as representative of the terrestrial humic-like FDOM, given the good linear correlation with $C2_{t\text{-}hum}$, in the upper 200 m (Table 3). The mixed layer (the dashed blue line in Figs. 6, 7 and 8 indicates the MLD) was well visible in the Tyrrhenian and Ionian Seas, whereas in the Algero-Provençal Basin, each station showed a different structure of the water column with a well-defined mixed layer visible only at station 13. The water column at stations 5 and 15 was almost completely mixed, while at station 11 stratification was weak (Figs. 6–8). The highest $Index_{str}$ (> 1 kg m^{-3}) was at stations 10, 11 and 13 and it progressively decreased moving toward the Gulf of Lions (station 15) and the Sardinian Channel (station 5) (Table 1).

Station 13, located in the westernmost part of the study area, was characterized by a MLD of 38 m and a DCM at 50 m (Fig. 6). In correspondence with the DCM, a decrease in $S_{275–295}$ (0.027 nm^{-1}) and a peak in both $C4_{m\text{-}hum}$ and $C5_{Trp}$ (Fig. 7) is visible. $C3_{t\text{-}hum}$ vertical profile was opposite to DOC, with low values in the upper 30 m, and an increase in correspondence with the thermocline (Fig. 8).

Station 11 showed a 2-stair thermocline with MLD of 38 and 86 m (Fig. 6). Chlorophyll showed two peaks at 36 and 87 m, but they are less marked than at station 13. A slight increase in DOC and a_{254} can be observed at about 50 m, whereas $C5_{Trp}$ showed a peak at both 50 and 100 m. $S_{275–295}$ slightly decreased at 100 m, in correspondence with the thermocline (Fig. 6).

Moving toward station 10, $Index_{str}$ decreased and MLD was 75 m. A general increase in chlorophyll was observed in the upper 50 m, without the formation of the DCM (Fig. 6). DOC showed the highest value in the surface sample and a progressive decrease in the mixed layer, to reach the lowest value (47 μM) at 150 m. The surface sample was characterized by high values of a_{254}, $C4_{m\text{-}hum}$ and $C5_{Trp}$ and a low value of $S_{275–295}$ (0.027 nm^{-1}). It is noteworthy the increase in both $C3_{t\text{-}hum}$ and $C4_{m\text{-}hum}$ below the mixed layer (Figs. 7 and 8).

Station 8 was characterized by low $Index_{str}$ (0.93 kg m^{-3}) and a MLD of 110 m (Table 1). A slight increase in chlorophyll was observed in the mixed layer, without the formation of the DCM. The high vertical mixing of the water column caused an almost uniform distribution of DOC, CDOM and FDOM in the mixed layer, excluding the peak in $C5_{Trp}$ observed at the surface (Fig. 7).

The upper 250 m of station 15 were completely mixed, as indicated by the $Index_{str}$ that is the lowest one observed in this study (0.30 kg m^{-3}) and the vertical profile of density that is almost vertical (Fig. 7). In the upper 50 m, chlorophyll showed the highest fluorescence. The high extent of vertical mixing can explain the low and almost homogenous values of DOC, $C3_{t\text{-}hum}$ and $C4_{m\text{-}hum}$. In the upper 75 m of this station, the values of $C3_{t\text{-}hum}$ (0.014–0.019 R.U.) and $C4_{m\text{-}hum}$ (0.018–0.022 R.U.) are the highest ones observed in this study (Figs. 7 and 8). Interestingly, compared to the other APB stations, $S_{275–295}$ showed the lowest values (0.024 nm^{-1}). This minimum was at ~20 m in correspondence with a peak in a_{254} and $C5_{Trp}$.

Station 5 was characterized by a low $Index_{str}$ (0.56 kg m^{-3}), a mixed layer deeper than 250 m and a DCM at 20 m (Fig. 6). DOC and a_{254} showed high values in the upper 100 m and no clear pattern in correspondence with DCM, whereas humic-like FDOM was almost constant.

Due to the sampling period (August 2010), the TS station was characterized by the highest $Index_{str}$ that resulted in (i) DOC and CDOM accumulation above the thermocline, (ii) a surface minimum of $C3_{t\text{-}hum}$ and $C4_{m\text{-}hum}$ and (iii) the highest $S_{275–295}$ value (0.040 nm^{-1}) (Figs. 6–8). A similar DOM dynamics was observed at the 3 stations located in the IS and sampled in November 2011, when the water column was well stratified. MLD was 35 m at station L119 and 50 m at both stations N1 and N2 (Table 1). DOC, CDOM and $C5_{Trp}$ accumulated in the mixed layer, where $C3_{t\text{-}hum}$ and $C4_{m\text{-}hum}$ showed their minimum and $S_{275–295}$ the highest values.

Table 5
Values of r^2 and p for the linear correlations among DOC, CDOM, FDOM and environmental parameters, taking into consideration all the samples.

	All samples																			
	Temp			AOU			Chl		DOC			a_{254}			a_{325}			$S_{275-295}$		
	0-Btm	0–200	200-Btm	0-Btm	0–200	200-Btm	0-100	0-Btm	0–200	200-Btm	0-Btm	0–200	200-Btm	0-Btm	0–200	200-Btm	0-Btm	0–200	200-Btm
Temp																			
AOU	*0.40***	*0.25***	0.12**																
Chl		–			–														
DOC	**0.68****	**0.60****	–	***0.65*****	***0.70*****	–	*0.19*	***0.80*****	*0.40***	–	***0.75*****	*0.35***	***0.62*****	*0.18***	***0.53*****	***0.48*****			
a_{254}	*0.43***	0.11	–	***0.67*****	***0.56*****	–	–	*0.41***	–	–	–	–	*0.15*	*0.21***	*0.35***	–	–	–	***0.62*****	–
a_{325}	*0.12***	–	–	*0.30***	–	–	0.13	–	*0.48***	–	–	–	0.12	*0.18***	0.25	–	*0.22***	–	***0.80*****	–
$S_{275-295}$	–	**0.50****	–	–	*0.17*	–	*0.14*	–	*0.22*	–	–	–	0.20	0.18**	–	–	–	*0.12*	***0.52*****	–
$C1_{PAH}$	–	*0.34***	–	–	011	–	0.19	–	***0.55*****	–	–	–	–	–	–	–	–	*0.13*	***0.49*****	–
$C2_{t\text{-}hum}$	*0.16***	***0.68*****	–	–	0.20	–	0.32	–	*0.49***	–	–	–	–	0.16**	0.11	–	–	–	–	–
$C3_{t\text{-}hum}$	*0.29***	***0.57*****	–	–	0.18	–	0.27	*0.11*	*0.41***	–	–	–	0.23**	–	*0.20*	–	–	–	–	–
$C4_{m\text{-}hum}$	–	*0.40***	–	–	0.13	–	*0.35***	–	–	–	–	0.15	–	–	–	–	–	–	–	–
$C5_{Trp}$	–	–	–	–	–	–	–	–	–	–	–									

Values of $r^2 < 0.1$ are not reported; values of $r^2 > 0.5$ are in bold.
** $p < 0.0001$. Negative correlations are indicated in italic. Btm = Bottom.

4. Discussion

4.1. CDOM in the Med Sea, a comparison with the oceans and the marginal seas

The data reported in this study are limited to the western Med Sea and the IS, with a gap in both the westernmost (e.g. Alboran Sea and Strait of Gibraltar) and easternmost areas. The range of a_{254} values well compare with data reported by Catalá et al. (2018) for the entire basin. The linear correlation between DOC and a_{254} is very similar to that reported by Catalá et al. (2018) (DOC = 9(± 1) + 46(± 1)·a_{254}; r^2 = 0.87, $p < 0.001$, n = 273), supporting that a_{254} can be considered representative of the CDOM dynamics on the basin scale. In contrast, in the ultra-oligotrophic Levantine Basin and in the deep IS, a_{325} is lower (0.05–0.15 m^{-1}) and $S_{275-295}$ is higher (0.030–0.045 nm^{-1}) than in our study (Fig. 4 in Catalá et al., 2018).

The comparison with studies focusing in coastal areas, or in marginal seas, shows that the CDOM absorption in open water of the Med Sea is generally lower than those observed in coastal areas impacted by river input (a_{280} = 0.95–2.3 m^{-1}) (Seritti et al., 1998; Vignudelli et al., 2004) and in the other marginal seas (Table 4). The values reported in our study are in the range of those reported for the oceans (Table 4). However, if we focus in the upper layer (0–100 m), a_{325} ranges between 0.18 and 0.33 m^{-1} in the Med Sea and between 0.02 and 0.15 m^{-1} in the oceans (Nelson and Siegel, 2013). Moving to dark open ocean, if only the data with AOU = 50–100 μM are taken into consideration, a_{325} ranged between 0.11 and 0.2 m^{-1} in the North Atlantic, with most of the samples with values of 0.12–0.14 m^{-1} and between 0.040 and 0.12 m^{-1} in the Pacific and Indian Oceans, respectively (Nelson et al., 2010, their Fig. 4). The comparison with our data (a_{325} = 0.07–0.24 m^{-1}) suggests that CDOM absorption in open water of the Western Med Sea and IS is generally higher than in Pacific and Indian Oceans (Nelson et al., 2010; Nelson and Siegel, 2013; Catalá et al., 2015), whereas it is similar to values observed in the North Atlantic, that receives considerable amount of terrestrial organic matter from the Arctic Ocean and the continents.

In the APB, TS and IS, $S_{275-295}$ is lower than in the open ocean (~0.04 nm^{-1}) (Aurin and Mannino, 2012) and in oligotrophic waters of the northern Gulf of Mexico (0.048 nm^{-1}) (Fichot and Benner, 2012), but in the range of values reported for the other marginal Seas (Table 4). In contrast, $SUVA_{254}$ is up to 4 times lower than those observed in the other marginal Seas (Table 4). The ratio between $S_{275-295}$ and $S_{350-400}$ (S_R), that is inversely related to the molecular weight of CDOM (Helms et al., 2008), is significantly lower than in the global ocean for the same range of AOU (Catalá et al., 2018). These results indicate that in the Med Sea, CDOM is characterized by molecules with an average molecular weight and aromaticity degree higher than in the open oceans, supporting the occurrence of a higher percentage of molecules with a terrestrial signature in this basin than in the open oceans.

4.2. FDOM characteristics in the Med Sea

The fluorescence PARAFAC components observed in this study well compare with the global ocean fluorescence inventories reported by Jørgensen et al. (2011) and Catalá et al. (2015, 2016) as well as with components found in the other marginal seas (Table 2), even if some differences can be highlighted. $C1_{PAH}$ from this study was not found in the open oceans, it matches with a component associated to ballast water (Murphy et al., 2006) and a component ($C4_{m\text{-}hum}$) dominating in harbors, the English Channel and in the Atlantic shelf approaching Delaware and Chesapeake Bay outflows and identified as PAHs substances (Murphy et al., 2008). The occurrence of a PAH-like component in the Med Sea is in agreement with the observation by Castro-Jiménez et al. (2012), that indicates an important net atmospheric input of PAHs to open sea waters of the WM and the IS. The robust linear correlation with $C2_{t\text{-}hum}$ (Table 3), supports that they have a common origin,

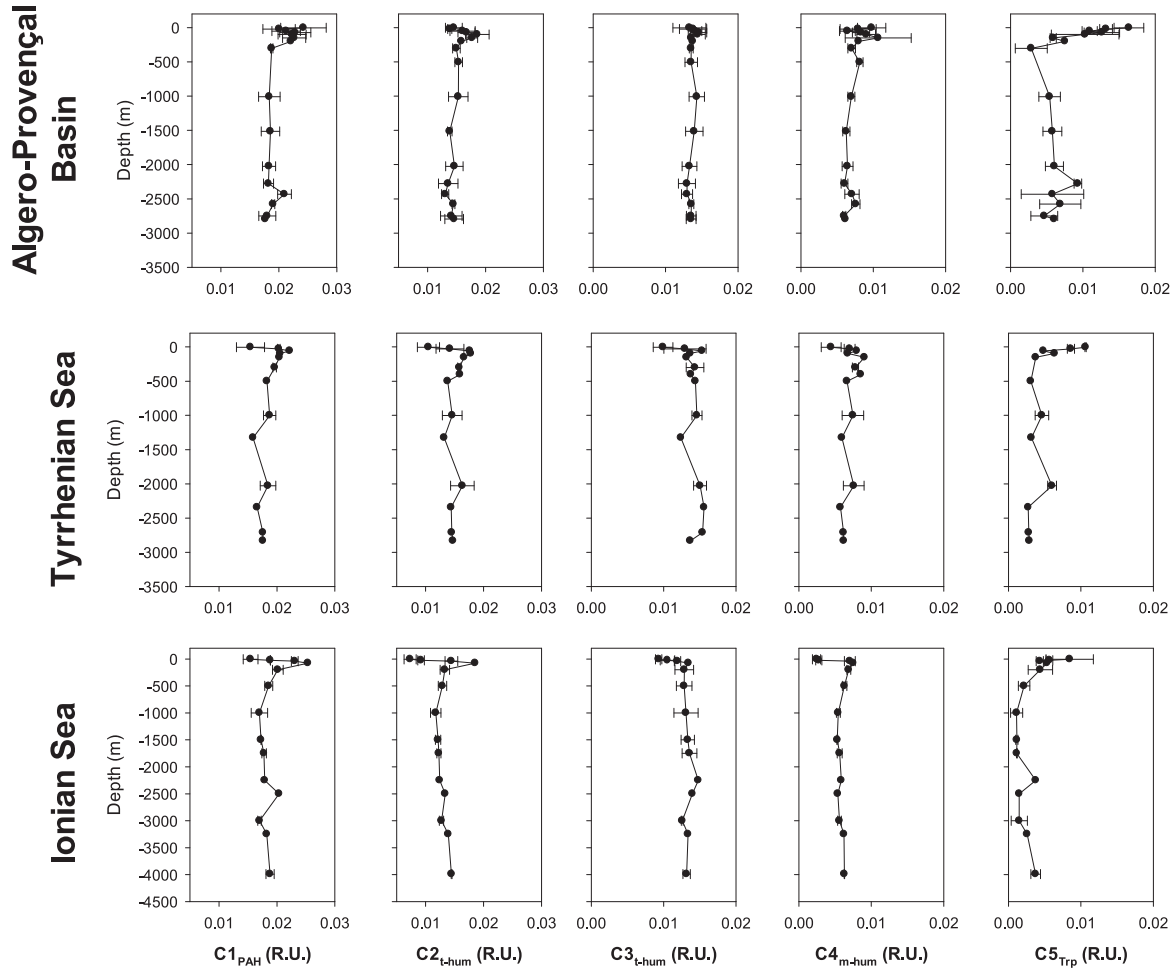

Fig. 5. Vertical profiles of mean values for the 5 components in the 3 areas. Error bars refer to the standard deviation among stations. The x-axes scale is different, in order to better represent the vertical profiles.

probably allocthonous. A similar component was found in the China and Okhotsk Seas (Table 2), but it was attributed to terrestrial humic-like FDOM. Comparative data and additional analysis are needed to confirm that component $C1_{PAH}$ can be a tracer of PAH pollutants.

A component with a such long wavelength emission maximum (516 nm) as $C3_{t\text{-}hum}$ has never been found in the open oceans. It is noteworthy that the wavelength of this emission maximum is typical of terrestrial humic acids characterized by either highly substituted aromatic nuclei or conjugated unsaturated systems capable of high degree of resonance. These characteristics suggest the presence of terrestrial molecules with a small degree of degradation (Senesi et al., 1989). A similar component was found in the Baltic, North and Black Seas (Table 2), supporting its strong terrestrial signature. The other terrestrial humic-like component ($C2_{t\text{-}hum}$), being similar to the terrestrial humic-like component found in the Black, China and Okhotsk Seas (Table 2), shows excitation and emission maxima shifted towards shorter wavelengths, suggesting that the Med Sea is characterized by a very complex, not degraded, terrestrial humic-like component ($C3_{t\text{-}hum}$) not observed in the open oceans and another one ($C2_{t\text{-}hum}$) more degraded than the terrestrial humic-like component found in oceanic waters.

In contrast to the main ocean basins and the Baltic, China and Okhotsk Seas, where between 2 and 4 protein-like components were observed, in the Med Sea our model found only 1 protein-like component ($C5_{Trp}$). The same applies for the Black Sea. There are evidences that protein-like substances are produced in-situ by phytoplankton and microbes (Stedmon and Markager, 2005b; Romera-Castillo et al., 2010; Zhao et al., 2017). In our study, the phenylalanine-like and tyrosine-like components were not found, in contrast to oceanic studies, that observed that the tyrosine-like fluorophores dominated in the open ocean waters (Mopper and Schultz, 1993; Yamashita et al., 2010b; Jørgensen et al., 2011). Our data suggest the predominance in the Med Sea of proteins containing Trp with respect to those containing only Tyr. The different protein composition could be explained by a different microbial community in the Med Sea, in agreement with the first data on marine microbe diversity, which indicate that prokaryotic assemblages are highly diverse, with the presence of bacterial and archaeal ecotypes, adapted to the unique hydrological, geological and geomorphological features of this basin (Luna, 2015).

The 5 components showed a different distribution within and below the mixed layer (Figs. 7–8), indicating that each component is affected by different processes leading to a change in the relative percentage of each component in the FDOM pool. The shape of vertical profiles of both humic-like and protein-like components well compare with those observed in the Atlantic, Pacific and Indian Oceans (Yamashita et al., 2010b; Jørgensen et al., 2011; Catalá et al., 2016). FDOM in the Med sea was dominated by humic-like components representing 70–95% and 65–100% of the total fluorescence in the upper 200 m and between 200 m and the bottom, respectively.

In the upper 200 m, DOC showed a significant ($p < 0.0001$) inverse relationship with $C2_{t\text{-}hum}$, $C3_{t\text{-}hum}$, and $C4_{m\text{-}hum}$, whereas no correlation was found with $C1_{PAH}$ and $C5_{Trp}$ (Table 5). In contrast to oceanic observations (Yamashita and Tanoue, 2009) a_{254} and a_{325} did not correlate with the 5 components (if we exclude the weak correlation between

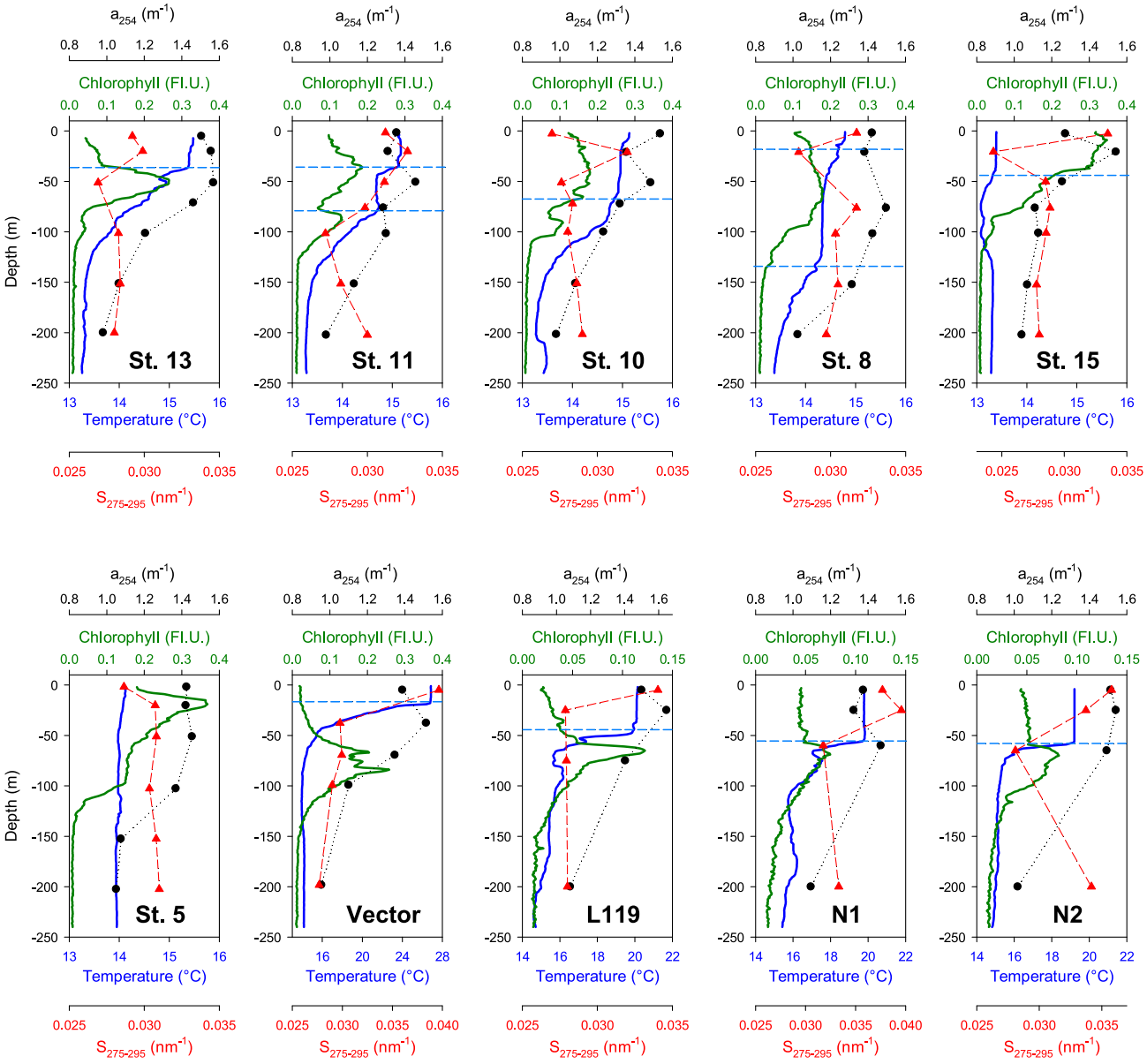

Fig. 6. Vertical profiles in the upper 250 m of temperature, chlorophyll, a_{254} and $S_{275–295}$ for each station. The dashed blue line is the mixed layer depth (MLD). The stations 5, 8, 10, 11, 13 and 15 are in the Algero-Provençal basin, the station Vector is in the Tyrrhenian Sea, and the N1, N2 and L119 stations are in the Ionian Sea. (For interpretation of the references to color in this figure legend, the reader is referred to the web version of this article.)

a_{325} and $C1_{PAH}$), neither taking into consideration all the data, nor focusing in the surface or in the deep waters (Table 5). These results indicate that in the Med Sea, CDOM and FDOM dynamics are decoupled and that absorption and fluorescence give information on different fractions of DOM. Interestingly, the robust correlation between $C4_{m\text{-}hum}$ and $C5_{Trp}$ (Table 3) below 200 m, indicates that the 2 components are coupled in the intermediate and deep waters, suggesting that both are produced in-situ even if no correlation with AOU was found. In the surface layer the removal processes are different, with photobleaching affecting $C4_{m\text{-}hum}$ more than $C5_{Trp}$ as suggested by the correlations with temperature (Table 5). Consumption rates higher than production rates could mask the relationship with AOU. The good correlation between $C2_{t\text{-}hum}$ and $C4_{m\text{-}hum}$ suggests that the 2 components are produced and removed by the same processes. A fraction of the marine humic-like substances could derive from the microbial transformation of terrestrial humic-like substances, or both components could be released in-situ by heterotrophic prokaryotes.

4.3. The main drivers of CDOM distribution in the surface layer (0–200 m)

Our data are in good agreement with the other Med Sea studies reporting a decoupling of CDOM dynamics between the surface layer, where CDOM dynamics is mainly explained by physical processes (sea surface temperature and photobleaching), and subsurface layer, where CDOM is mainly driven by biological processes (phytoplankton release and/or microbial transformation) (Bracchini et al., 2010; Organelli et al., 2014; Xing et al., 2014; Pérez et al., 2016). However, in these papers no FDOM data is reported. Our study unveils that this decoupling is even more clear when the FDOM components are taken into consideration and highlights that the PARAFAC components are differently affected by physical and biological processes. In the APB, samples were collected at the beginning of spring; this season is characterized by the initial phase of the phytoplankton bloom, as supported by the high chlorophyll fluorescence (Fig. 6), and by a high extent of vertical mixing, as supported by the low $Index_{str}$ (Table 1) and the

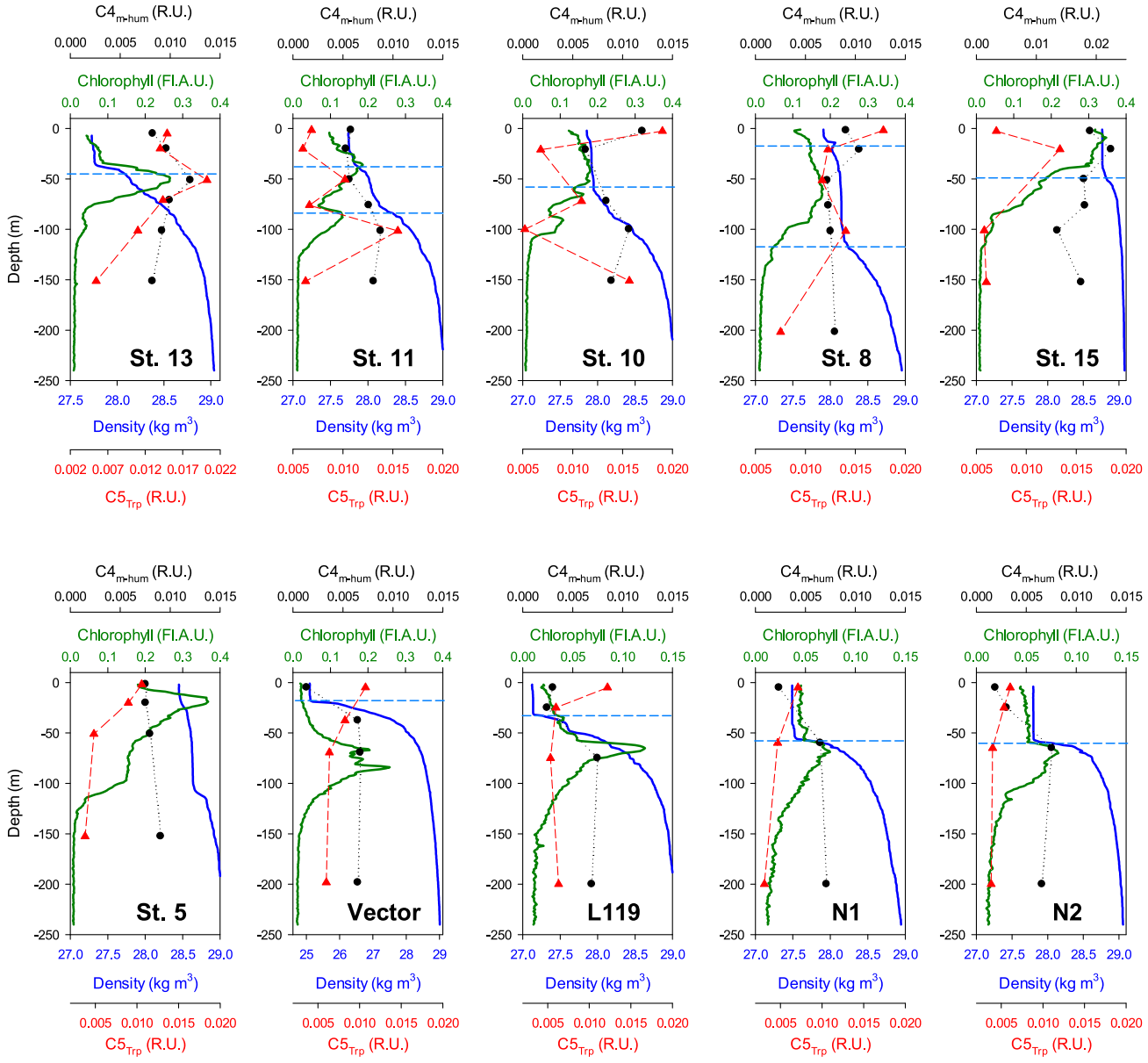

Fig. 7. Vertical profiles of density, chlorophyll, $C4_{m\text{-}hum}$ and $C5_{Trp}$ for each station. The dashed blue line is the mixed layer depth (MLD). The stations 5, 8, 10, 11, 13 and 15 are in the Algero-Provençal basin, the station Vector is in the Tyrrhenian Sea, and the N1, N2 and L119 stations are in the Ionian Sea. (For interpretation of the references to color in this figure legend, the reader is referred to the web version of this article.)

vertical profiles of both temperature and density (Figs. 6 and 7). In contrast, in the TS and IS, samples were collected in August and November, respectively, when the water column is highly stratified (Table 1, Fig. 6). We therefore expect that different processes are the main drivers of DOC, CDOM an FDOM dynamics in the 3 areas/periods.

4.3.1. CDOM and FDOM release by phytoplankton and/or bacterioplankton

In most of the APB stations a decrease in $S_{275–295}$ and an increase in $C5_{Trp}$ and $C4_{m\text{-}hum}$ was observed in correspondence with the DCM (high chlorophyll values) (Figs. 6 and 7), whereas no clear pattern was observed for a_{254} (excluding station 15) or for DOC (Figs. 6 and 8). At some stations (e.g. Station 10) a minimum in $S_{275–295}$ in correspondence with high values of a_{254}, $C5_{Trp}$ and $C4_{m\text{-}hum}$ was observed in the surface sample. The low values of $S_{275–295}$ in correspondence with high values of $C5_{Trp}$ and $C4_{m\text{-}hum}$ can be a clear indication of FDOM in-situ production, since microbial activity counteracts the photobleaching effect increasing the molecular weight and aromaticity (Helms et al., 2008; Catalá et al., 2015; Maqbool et al., 2017). A peak in protein-like FDOM in correspondence with DCM was observed in the oceans (Catalá et al., 2016), whereas a peak in CDOM together with a decrease in S was observed few meters above the DCM in the Sargasso Sea (Nelson et al., 2004), at the Boussole site in spring and summer (a_{442}, Organelli et al., 2014), in the northwestern Med Sea in September 2011 and May 2012 (a_{320}, Pérez et al., 2016) and in the Ionian Sea in November 2004 (a_{300}, Bracchini et al., 2010). In both the northwestern and eastern Med Sea, absorption data at 412 nm (a_{412}), estimated from fluorometric and radiometric measurements of “Bio-Argo” floats, showed a sub-surface maximum of a_{412} in correspondence with the DCM in fall, whereas in winter and early spring it deepened following the MLD (Xing et al., 2014). The low sampling frequency in the upper 200 m prevents knowing the exact position of the CDOM/FDOM peak in our data; we cannot therefore exclude that it is few meters above the DCM. The peak in $C5_{Trp}$ and $C4_{m\text{-}hum}$ in proximity of the DCM supports that phytoplankton and/or bacterioplankton actively growing release both humic-like and protein-like substances as widely documented (Romera-Castillo

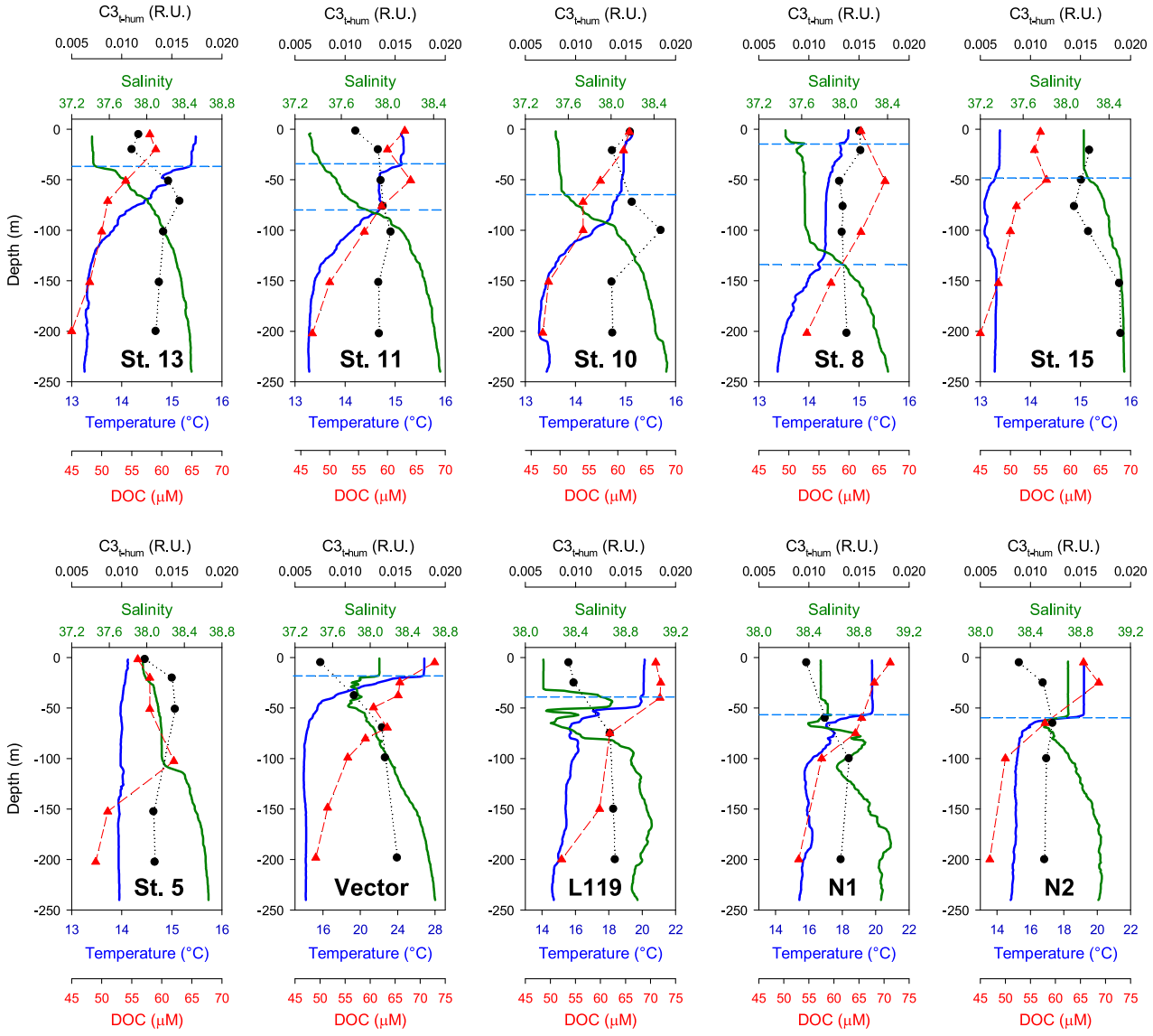

Fig. 8. Vertical profiles of Temperature, Salinity, DOC and $C3_{t\text{-}hum}$, for each station. The dashed blue line is the mixed layer depth (MLD). The stations 5, 8, 10, 11, 13 and 15 are in the Algero-Provençal basin, the station Vector is in the Tyrrhenian Sea, and the N1, N2 and L119 stations are in the Ionian Sea. (For interpretation of the references to color in this figure legend, the reader is referred to the web version of this article.)

et al., 2010, 2011; Lønborg et al., 2015; Zhao et al., 2017) and that these components are not immediately removed and accumulate. The direct production of recalcitrant DOM with a chromophoric signature and of recalcitrant humic-like FDOM by bacterioplankton has been observed in the oceans (Nelson et al., 2004; Yamashita and Tanoue, 2008; Romera-Castillo et al., 2011; Jørgensen et al., 2014; Lønborg et al., 2015). The peak in FDOM can be explained not only through the direct release of recalcitrant FDOM but also through bacterial transformation of the labile DOM into recalcitrant FDOM in agreement with the model of the microbial carbon pump (Jiao et al., 2010).

No correlation was observed between chlorophyll and DOC, CDOM or FDOM (Table 5), even when only samples collected in the APB are taken into consideration (Table 6), in agreement with results from open ocean waters (Jørgensen et al., 2011). The time shift between chlorophyll maximum and CDOM accumulation (Nelson et al., 2004; Organelli et al., 2014; Xing et al., 2014) may prevent finding a direct relationship in our data. Time-series of CDOM, FDOM, chlorophyll and prokaryotic heterotrophs abundance are therefore mandatory to investigate the direct release of DOM by phytoplankton or its transformation by microbes. When only the data collected in the upper 100 m of the IS (November) are taken into consideration, a very good inverse correlation is observed between chlorophyll and both temperature and DOC; in addition chlorophyll directly correlates with all the humic-like components (Table 8). This correlation suggests a direct production of FDOM by phytoplankton, even if a negative effect of temperature on both FDOM (photobleaching) and phytoplankton (photo-acclimation of intracellular chlorophyll concentration together with nutrient limitation) cannot be excluded.

It is noteworthy that in the Gulf of Lions (WM, station 15, Fig. 1), the most productive area of the Med Sea, surface fluorescence intensities of $C4_{m\text{-}hum}$ (marine humic-like) are significantly higher (2.6-fold, $p < 0.05$) than in all the other stations. The increase in $C4_{m\text{-}hum}$ can be explained by the input of nutrients that induces the phytoplankton bloom and an increase in microbial productivity, as observed in upwelling regions of the oceans (Nieto-Cid et al., 2005), as well as by the uplifting of water with higher values of humic-like FDOM from deeper layers (Siegel et al., 2002; Catalá et al., 2016).

In the surface layer, the robust linear inverse correlation between AOU, used as a proxy for microbial mineralization, and both DOC ($r^2 = 0.70$) and a_{254} ($r^2 = 0.56$) (Table 5; Fig. 9) indicates that microbial

Table 6
Values of r^2 and p for the linear correlations among DOC, CDOM, FDOM and environmental parameters in the Algero-Provencal Basin.

	Algero-Provencal Basin																		
	Temp			AOU			Chl	DOC			a_{254}			a_{325}			$S_{275–295}$		
	0-Btm	0–200	200-Btm	0-Btm	0–200	200-Btm	0-100	0-Btm	0–200	200-Btm	0-Btm	0–200	200-Btm	0-Btm	0–200	200-Btm	0-Btm	0–200	200-Btm
Temp																			
AOU	*0.23***	*0.38**	**0.79****																
Chl		*0.33**																	
DOC	**0.78****	**0.52****	0.26**	*0.34***	***0.68****	–	–												
a_{254}	**0.76****	**0.51****	–	*0.45***	*0.45**	–	–	**0.78****	0.41*	–									
a_{325}	**0.60****	0.46**	–	*0.27***	*0.20**	–	–	**0.55****	0.12*	–	**0.88****	**0.71****	**0.60****						
$S_{275–295}$	–	–	–	–	–	–	–	–	0.23*	0.20*	–	–	*0.23**	*0.27***	*0.17**	***0.58****			
$C1_{PAH}$	–	–	–	–	–	–	0.14	–	–	–	0.12*	–	–	0.14*	0.15*	–	–	*0.41**	–
$C2_{t\text{-}hum}$	–	0.15*	–	–	0.11	–	0.33*	–	*0.30**	–	0.18*	–	–	0.30**	–	–	*0.18**	***0.70****	–
$C3_{t\text{-}hum}$	–	*0.12**	–	–	–	–	0.19*	–	*0.16**	–	–	–	–	–	–	–	–	*0.23**	–
$C4_{m\text{-}hum}$	–	*0.28**	–	–	–	–	0.30*	–	*0.15**	–	–	–	–	0.12*	–	–	–	*0.36**	–
$C5_{Trp}$	–	0.13*	–	–	–	–	–	–	–	–	–	0.41	–	–	0.43*	*0.12**	–	–	–

Values of $r^2 < 0.1$ are not reported; values of $r^2 > 0.5$ are in bold. *$p < 0.05$; **$p < 0.0001$. Negative correlations are indicated in italic. Btm = Bottom.

Table 7
Values of r^2 and p for the linear correlations among DOC, CDOM, FDOM and environmental parameters in the Tyrrhenian Sea.

	Tyrrhenian Sea (TS)																		
	Temp			AOU			Chl	DOC			a_{254}			a_{325}			$S_{275–295}$		
	0-Btm	0–200	200-Btm	0-Btm	0–200	200-Btm	0-100	0-Btm	0–200	200-Btm	0-Btm	0–200	200-Btm	0-Btm	0–200	200-Btm	0-Btm	0–200	200-Btm
Temp							–												
AOU	*0.22**	–	0.33*				*0.15*												
Chl		*0.32**			*0.15*														
DOC	0.45**	**0.54***	0.42*	***0.72****	***0.85****	**0.63****	*0.34**												
a_{254}	0.16*	–	0.16	***0.83****	***0.69****	–	–	**0.72****	–	–									
a_{325}	–	*0.38**	0.23*	***0.70****	*0.49**	–	–	0.37*	–	–	**0.77****	0.23	**0.66****						
$S_{275–295}$	0.34	**0.78***	–	–	–	–	–	0.19*	0.42*	–	–	–	*0.13*	–	***0.67****	***0.60****			
$C1_{PAH}$	*0.39*	***0.93****	0.21	***0.50****	–	–	0.15	0.42*	*0.48*	*0.12*	–	–	**0.62***	0.34*	**0.58***	0.18	*0.23**	***0.89****	–
$C2_{t\text{-}hum}$	***0.67****	***0.95****	–	*0.28**	–	***0.63****	0.28	–	***0.57****	*0.13*	–	–	0.46*	–	0.35	0.12	*0.32**	***0.73****	–
$C3_{t\text{-}hum}$	***0.70****	***0.78****	–	–	–	–	**0.60***	*0.17**	*0.44*	–	*0.17**	–	–	–	0.22	–	0.14	*0.44*	–
$C4_{m\text{-}hum}$	***0.57***	***0.92****	–	–	–	*0.26*	0.29	*0.41**	***0.81****	–	–	–	**0.75***	–	0.21	0.35*	*0.37**	***0.74****	–
$C5_{Trp}$	–	0.14	–	–	–	–	–	*0.18**	0.16	–	–	0.17	0.26*	–	–	–	–	–	–

Values of $r^2 < 0.1$ are not reported; values of $r^2 > 0.5$ are in bold. *$p < 0.05$; **$p < 0.0001$. Negative correlations are indicated in italic. Btm = Bottom.

Table 8
Values of r^2 and p for the linear correlations among DOC, CDOM, FDOM and environmental parameters in the Ionian Sea.

	Ionian Sea (IS)																			
	Temp			AOU		Chl	DOC		a_{254}			a_{325}			$S_{275-295}$				
	0-Btm	0–200	200-Btm	0-Btm	0–200	200-Btm	0-100	0-Btm	0–200	200-Btm	0-Btm	0–200	200-Btm	0-Btm	0–200	200-Btm	0-Btm	0–200	200-Btm	
Temp																				
AOU	***0.91***	***0.75***	–																	
Chl		***0.83***			0.30															
DOC	***0.93***	***0.86***	0.13*	***0.96***	***0.85***	***0.57***	***0.75***													
a_{254}	***0.85***	0.48*	0.14	***0.93***	***0.77***	*0.17**	–	***0.93***	***0.67***	0.33*										
a_{325}	0.24*	–	–	*0.32**	–	–	–	0.39*	–	0.13	***0.60***	0.17	***0.67***							
$S_{275-295}$	0.21*	0.16	–	*0.18**	–	–	–	0.11*	–	–	–	–	*0.13*	–	***0.75***	***0.50***				
$C1_{PAH}$	–	*0.34**	–	–	0.13	*0.14**	***0.54***	–	–	0.28*	–	–	0.19	0.35*	0.35*	–	–	***0.58***	–	
$C2_{t\text{-}hum}$	*0.33**	***0.63***	–	0.25*	0.32	*0.39**	***0.70***	*0.14**	*0.27*	0.23*	–	–	0.21*	–	0.11	–	*0.20**	*0.40**	–	
$C3_{t\text{-}hum}$	***0.63***	***0.71***	–	***0.52***	0.47*	–	***0.72***	***0.48***	*0.41**	–	*0.43**	*0.26*	–	–	–	–	*0.13**	*0.27*	–	
$C4_{m\text{-}hum}$	*0.41**	***0.79***	0.11	0.43*	***0.67***	–	***0.68***	***0.24***	***0.55***	0.28*	*0.15**	*0.26*	***0.52***	–	–	0.19	*0.14**	*0.21*	–	
$C5_{Trp}$	***0.65***	0.24	–	***0.66***	*0.19*	*0.14*	*0.43*	***0.69***	0.32	0.23*	**0.60**	–	0.23*	0.26*	–	–	–	–	–	

Values of $r^2 < 0.1$ are not reported; values of $r^2 > 0.5$ are in bold. $^*p < 0.05$; $^{**}p < 0.0001$. Negative correlations are indicated in *italic*. For chlorophyll, only the values collected in the upper 100 m were taken into consideration. Btm = Bottom.

removal is the main processes affecting DOC and CDOM dynamics and it can explain up to 70% of DOC and 55% of CDOM decrease in the upper 200 m, in agreement with the results by Catalá et al. (2018). No significant correlation was observed between FDOM and AOU (Table 5), suggesting that in the Med Sea photobleaching is the main process affecting FDOM dynamics in the surface layer.

4.3.2. Photobleaching

In both the TS and IS, the high extent of vertical stratification favors the accumulation of DOM in the mixed layer making photobleaching the main process affecting CDOM and FDOM dynamics. A robust power law correlation was observed between temperature and $C2_{t\text{-}hum}$, $C3_{t\text{-}hum}$ and $C4_{m\text{-}hum}$ (Fig. 10). A good linear correlation was also observed between temperature and DOC (Fig. 10), whereas no correlation was observed between temperature and CDOM or $C5_{Trp}$ (Table 5).

Temperature does not affect directly DOM, but it can be considered as a tracer of different processes that can impact DOM dynamics. Higher temperatures are indicators of a higher degree of stratification and therefore of a more prolonged exposure to solar radiation, leading to photodegradation. No correlation was found between temperature and chlorophyll, supporting that temperature is mainly an indicator of photobleaching and stratification. The robust direct correlation between temperature and DOC ($r^2 = 0.60$, Table 5) supports that DOC accumulates in warm waters, in agreement with observations previously reported for the Med Sea (Santinelli et al., 2013), whereas the inverse correlation with FDOM (Table 5) indicates that photobleaching affects both terrestrial and marine humic-like components, as observed by Xing et al. (2014) and Catalá et al. (2018). As expected, this correlation was not found in the APB (Table 6), and strongly improves in the TS (Table 7) and IS (Table 8). A robust linear correlation was also observed between temperature and $S_{275–295}$ (Table 5), supporting the occurrence of the smallest molecules produced by photodegradation in the warmest water (Helms et al., 2008). These data support that photodegradation represents the main removal mechanism for humic-like substances and controls CDOM abundance in the surface ocean, whereas its impact on protein-like substances is lower (Bracchini et al., 2010; Nelson et al., 2010, 2007; Nelson and Siegel, 2013; Stedmon and Markager, 2005b; Vodacek et al., 1997; Yamashita et al., 2010b). The microbial degradation of humic-like FDOM cannot be excluded, even if it is not considered a major sink (Stedmon and Markager, 2005b) as suggested by the weak correlation between AOU and FDOM (Table 5). The minimum in $C1_{PAH}$ observed in the photic zone, together with the good inverse correlation with temperature, indicates that $C1_{PAH}$ is mainly removed by photodegradation. The lack of correlation with AOU suggests that biological processes are not affecting this component in contrast to results by Castro-Jiménez et al. (2012), reporting that degradation processes by zooplankton and bacteria represent an additional sink for PAHs, especially for the low molecular weight (LMW).

4.4. The main drivers of DOM distribution in deep waters

In the deep open ocean and marginal seas, the fluorescence intensity of humic-like substances correlates positively with AOU (Hayase and Shinozuka, 1995; Yamashita et al., 2007, 2008; Yamashita and Tanoue, 2008, 2009; Jørgensen et al., 2011; Nelson et al., 2010; Nelson and Siegel, 2013; Catalá et al., 2015) or with Apparent Carbon Mineralization (ACM) (Margolin et al., 2018), suggesting that when organic matter, mainly coming from sinking particles, is oxidized a fluorescent by-product is formed. In the Med Sea, a_{254}, and DOC showed a robust inverse linear correlation with AOU ($a_{254} = 1.45(\pm 0.03) - 0.008(\pm 0.0006)\cdot AOU$; $r^2 = 0.67$, $p < 0.0001$, $n = 109$; $DOC = 63(\pm 1) - 0.3(\pm 0.02)\cdot AOU$; $r^2 = 0.65$, $p < 0.0001$; $n = 172$); a weaker but significant correlation was also observed with a_{325} (Table 5). The correlation is lost when the data collected in the upper 200 m are excluded from the regression. This finding is in contrast to oceanic observations reporting a direct

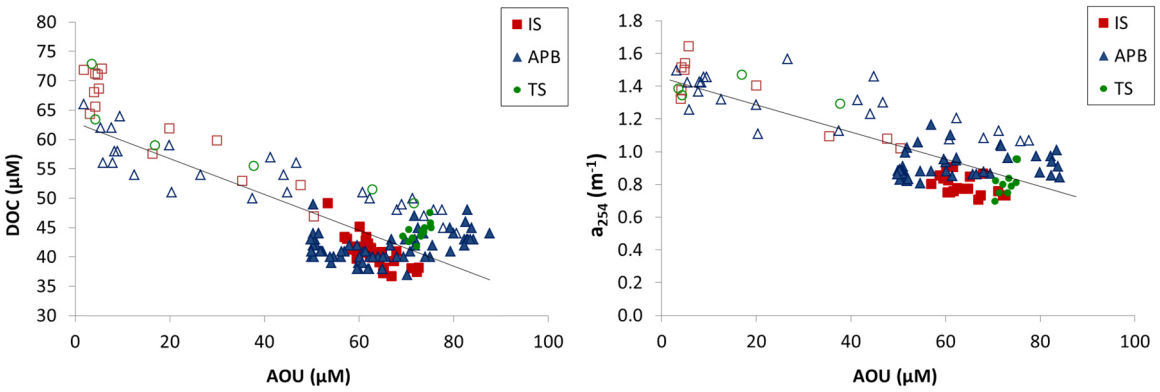

Fig. 9. Correlation between DOC and AOU (on the left) and between a_{254} and AOU (on the right). Empty symbols refer to samples collected in the upper 200 m, filled symbols to samples collected between 200 m and the bottom.

correlation between a_{325} and AOU. This apparent inconsistency can be solved looking at the value of AOU. In our study the maximum value of AOU is 88 µM, whereas in the oceans AOU is up to 300 µM. Looking at the relationship reported by Nelson et al. (2010) it is clear that if only the data with AOU < 100 µM were taken into consideration no relationship would have been found, even in the oceans. This observation suggests that the production of FDOM in deep waters mainly occurs when AOU is > 100 µM, that is in deep waters older than those found in the Med Sea or in waters where oxidation processes removed all the oxygen, leading to anoxia as in the Black Sea (Margolin et al., 2018). The low sinking POC fluxes characteristics of the Med Sea (Speicher et al., 2006), can help to explain the absence of the correlation.

These data indicate that in the dark Med Sea, there is not a net in-situ production of humic-like FDOM by microbial mineralization (lack of correlation with AOU). Even if humic-like FDOM can be produced in the surface layer by phytoplankton and heterotrophic prokaryotes, we think that external sources and general circulation could play a major role in determining CDOM distribution in deep waters (Nelson et al., 2007, 2010; Jørgensen et al., 2011; Nelson and Siegel, 2013; Catalá et al., 2015) in agreement with radiocarbon data (Santinelli et al., 2015) and the recalcitrant signature of FDOM associated with atmospheric aerosol (Sánchez-Pérez et al., 2016). Finally, chemosynthesis or POC dissolution could represent production mechanisms of $C5_{Trp}$ in deep waters, explaining the increase around 2000 m observed in the 3 areas (Fig. 5). Further studies are mandatory to confirm this hypothesis.

4.5. The Med Sea: a marginal basin with biogeochemical characteristics similar to the oceans

The Med Sea is the largest marginal basin in the world. It has a high coastline to surface ratio and it is connected with the oceans through the Gibraltar Strait (286 m maximum depth and 14 km width) (De Stephanis et al., 2008). It does have a high value of drainage area to surface area compared to the open ocean. Despite being a marginal basin it has less "terrestrial" characteristics than the other marginal basins (Table 4), since it has a large volume ($3.75{\cdot}10^6$ km^3), its continental shelves are narrow and it is a concentration basin, meaning that evaporation is higher than precipitations and run off. It is therefore the only marginal basin characterized by salinity higher than the oceans (Table 4) and stock of nutrients much lower than the other marginal basins and even lower than the oceans (Ribera d'Alcalà et al., 2003). It also features an anti-estuarine circulation, meaning that all the waters entering in the surface layer recirculate in the intermediate and deep layer before exiting the basin, with residence time of waters much longer than the other marginal basins, where the circulation is estuarine and all the water entering the surface layer exits from the surface layer. These peculiarities reflect in DOC concentrations almost identical to those reported for oceanic waters (Hansell, 2002; Hansell et al., 2009; Carlson et al., 2010; Hansell and Carlson, 2013), but much lower than those observed in the other marginal Seas (Table 4). DOM dynamics in the Med Sea well compare with the oceanic one, despite terrestrial inputs are expected to affect DOM dynamics to a larger extent than in the open ocean. Even though the Med Sea behaves as a miniature ocean for DOC concentrations and its distribution, its composition shows some intriguing differences, supported by radiocarbon (Santinelli et al., 2015) and Fourier Transform Ion Cyclotron Resonance mass spectroscopy (FT-ICR-MS) data (Martínez-Pérez et al., 2017a). These papers suggest that DOM in the Med Sea is older, lighter and with a higher degradation index than the DOM coming from the Atlantic Ocean.

Optical properties support the different DOM composition with respect to the oceans and suggest some differences with respect to the other marginal basins, opening intriguing questions about the source

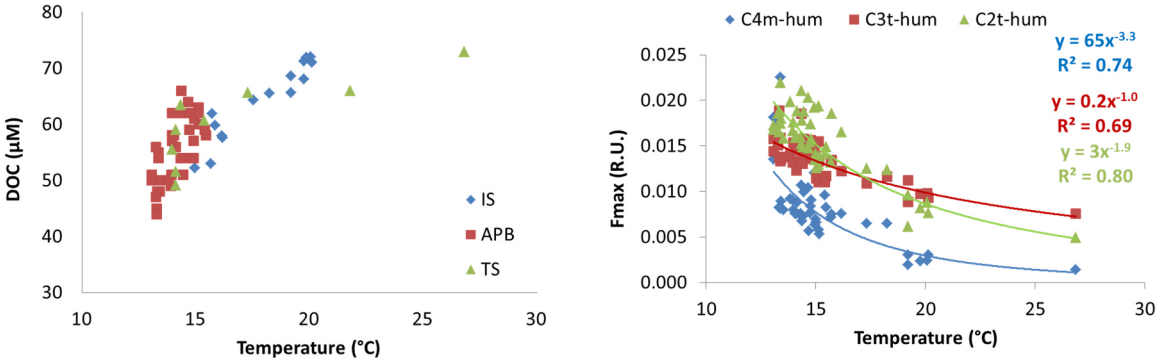

Fig. 10. Correlation between temperature and DOC (on the left) and between temperature and the 3 humic-like components (on the right).

and cycle of allocthonous molecules in the open sea waters of the Med Sea. The data reported in this paper support the hypothesis that a larger fraction of DOM is chromophoric and characterized by a larger percentage of humic-like substances than in the open oceans. The external sources of DOM to the Med Sea are rivers, atmosphere and groundwaters. Unfortunately, a direct comparison of CDOM input from external sources between the Med Sea, the oceans and the other marginal seas is very difficult to make due to the lack of CDOM data. In the following paragraph we therefore report a comparison of DOC fluxes from rivers and the atmosphere between the Med Sea and the oceans assuming that a similar fraction of DOC coming from these sources is composed by chromophoric molecules. While these assumptions can be valid for the riverine DOM, we expect that a higher fraction of atmospheric DOM is composed by chromophoric molecules in the Med Sea than in the ocean, due to the smaller size, higher urbanization degree of this basin and the higher impact of Saharan dust deposition events.

The most recent estimate of river input of DOC to the Med Sea indicates a total flux of $0.644–0.712 \cdot 10^{12}$ g DOC y^{-1} (Santinelli et al., 2015). The total DOC input from the rivers, divided by the entire volume of the basin ($3.75 \cdot 10^{6}$ km^3), suggests a contribution of $0.17–0.19 \cdot 10^{6}$ g DOC y^{-1} km^{-3}, assuming that terrestrial DOC is not removed. This value is comparable to that estimated for the global ocean ($0.14–0.18 \cdot 10^{6}$ g DOC y^{-1} km^{-3}), suggesting that even if rivers can be an important source of terrestrial DOM, they are not enough to explain the richness in humic-like molecules observed in the Med Sea.

Data on wet and dry DOC depositions from the atmosphere are scarce for the Med Sea and limited to specific areas (De Vicente et al., 2012; Djaoudi et al., 2018; Economou and Mihalopoulos, 2002; Pulido-Villena et al., 2008). In order to have a regional estimate of the total (wet + dry) atmospheric input of DOC, the annual average DOC flux (0.14–0.42 mmol m^{-2} d^{-1}) was multiplied by the Med Sea area ($2.5 \cdot 10^{6}$ km^2) (for further details refer to Santinelli, 2015). This calculation indicates a flux of $1.5–4.6 \cdot 10^{12}$ g DOC y^{-1} suggesting that atmospheric input can be 2–6 fold larger than river input. The global estimation for wet atmospheric DOC deposition to the global ocean is $90–246 \cdot 10^{12}$ g DOC y^{-1} (Willey et al., 2000; Kanakidou et al., 2012) and $1.5 \cdot 10^{12}$ g DOC y^{-1} to the Med Sea (Economou and Mihalopoulos, 2002). If these fluxes are normalized by the volume of the water, we obtain that atmospheric input accounts for $4 \cdot 10^{5}$ g DOC $y^{-1}km^{-3}$ in the Med Sea and $0.7–1.8 \cdot 10^{5}$ g DOC y^{-1} km^{-3} in the oceans. These values are 2–5 times larger in the Med Sea than in the oceans, suggesting that atmosphere can be the main source of allocthonous DOM to the Med Sea, thus explaining its richness in humic-like substances. In contrast to results from the North Atlantic (Jørgensen et al., 2011), no correlation was found between salinity and terrestrial humic-like FDOM below 200 m, further supporting that rivers are not the main source of terrestrial humic-like FDOM to the Med Sea. However it cannot be excluded that terrestrial FDOM is transformed, mixed and transported by water masses circulation, masking the correlation.

The idea that atmosphere can be the major source of allocthonous DOM to the Med Sea is also in agreement with the observations by Sánchez-Pérez et al. (2016), who collected a 2-year time series data on FDOM deposition in the Northwestern Med Sea and showed that aerosol deposition induced an increase in the proportion of FDOM in the DOM pool.

5. Conclusions

The data on DOC and optical properties (both absorption and fluorescence) of CDOM reported in this study support that the Med Sea behaves as a miniature ocean for DOC concentrations and distribution, whereas its chromophoric pool shows peculiariaties. CDOM absorption in the western Med Sea and IS is generally lower than those observed in the other marginal seas, but higher than in the oceans. The fluorescence PARAFAC components show some differences with both the oceans and the marginal seas. The PAH-like ($C1_{PAH}$) and terrestrial humic-like ($C3_{t\text{-}hum}$) component were found in other marginal basins but not in the open oceans. In contrast to the oceans and most of the marginal seas, only one protein-like component was found, opening intriguing questions about the role of microbial communities in its production and removal in the Med Sea. Interestingly, net production of humic-like FDOM as function of mineralization was not observed in the intermediate and deep waters of the Med Sea. The observation that DOM pool in the Med Sea is dominated by humic-like substances with an allocthonous origin opens intriguing questions about the impact of external sources of DOM to the basin.

Our data confirm that a_{254} can be a good proxy for DOC in the Med Sea and that in the surface layer photobleaching plays a relevant role in the removal of humic-like fluorescence. The release of both protein-like and humic-like substances occurs in proximity of the DCM. Additional data on microbial communities and DOM molecular composition as well as additional studies combining different approaches (in-situ data, incubation experiments, modelling effort) are mandatory to unveil the fascinating DOM dynamics in the Med Sea. The few information available on CDOM and FDOM input from external sources hinders an estimate of their relative importance and require further research.

Acknowledgments

This research was supported by PERSEUS project, Funded by the EU under FP7 Theme “Oceans of Tomorrow” OCEAN.2011-3 and by the Italian Flagship project RITMARE funded by the Italian Ministry of Research and University. Most of the samples were collected in March/April 2008 during the cruise S-IT4, carried out in the framework of the European IP Project SESAME (Southern European Seas Assessing and Modelling Ecosystem changes). CTD and oxygen data were kindly provided by K. Schroeder and M. Borghini (CNR-ISMAR), by M. Sprovieri (CNR-IAMC), F. Conversano (SZN) and by E. Zambianchi (Università Parthenope). We also thank the 3 anonymous reviewers for their helpful suggestions and comments.

Appendix A. Supporting information

Supplementary data associated with this article can be found in the online version at doi:10.1016/j.dsr.2019.01.007.

References

Antoine, D., d'Ortenzio, F., Hooker, S.B., Bécu, G., Gentili, B., Tailliez, D., Scott, A.J., 2008. Assessment of uncertainty in the ocean reflectance determined by three satellite ocean color sensors (MERIS, SeaWiFS and MODIS-A) at an offshore site in the Mediterranean Sea (BOUSSOLE project). J. Geophys. Res.: Oceans 113 (C7). https://doi.org/10.1029/2007JC004472.

Aurin, D., Mannino, A., 2012. A database for developing global ocean color algorithms for colored dissolved organic material, CDOM spectral slope, and dissolved organic carbon. In Paper presented at Ocean Optics XXI, 8–12 October 2012, The Oceanography Society, Glasgow, UK.

Benson, B.B., Krause Jr., D., 1984. The concentration and isotopic fractionation of oxygen dissolved in freshwater and seawater in equilibrium with the atmosphere 1. Limnol. Oceanogr. 29 (3), 620–632. https://doi.org/10.4319/lo.1984.29.3.0620.

Bracchini, L., Tognazzi, A., Dattilo, A.M., Decembrini, F., Rossi, C., Loiselle, S.A., 2010. Sensitivity analysis of CDOM spectral slope in artificial and natural samples: an application in the central eastern Mediterranean Basin. Aquat. Sci. 72 (4), 485–498. https://doi.org/10.1007/s00027-010-0150-y.

Bricaud, A., Morel, A., Prieur, L., 1981. Absorption by dissolved organic matter of the sea (yellow substance) in the UV and visible domains. Limnol. Oceanogr. 26 (1), 43–53. https://doi.org/10.4319/lo.1981.26.1.0043.

Cárdenas, C.S., Gerea, M., Garcia, P.E., Pérez, G.L., Diéguez, M.C., Rapacioli, R., Reissig, M., Queimaliños, C., 2017. Interplay between climate and hydrogeomorphic features and their effect on the seasonal variation of dissolved organic matter in shallow temperate lakes of the Southern Andes (Patagonia, Argentina): a field study based on optical properties. Ecohydrology. https://doi.org/10.1002/eco.1872.

Carlson, R.E., Fritsch, F.N., 1989. An algorithm for monotone piecewise bicubic interpolation. SIAM J. Numer. Anal. 26 (1), 230–238. https://doi.org/10.1137/0726013.

Carlson, C.A., Hansell, D.A., Nelson, N.B., Siegel, D.A., Smethie, W.M., Khatiwala, S., Meyers, M.M., Halewood, E., 2010. Dissolved organic carbon export and subsequent remineralization in the mesopelagic and bathypelagic realms of the North Atlantic basin. Deep Sea Res. Part II: Top. Stud. Oceanogr. 57 (16), 1433–1445. https://doi.org/10.1016/j.dsr2.2010.02.013.

Carlson, C.A., Hansell, D.A., 2015. DOM sources, sinks, reactivity, and budgets. In Biogeochemistry of Marine Dissolved Organic Matter (Second Edition) pp. 65–126. https://doi.org/10.1016/B978-0-12-405940-5.00003-0.
Castro-Jiménez, J., Berrojalbiz, N., Wollgast, J., Dachs, J., 2012. Polycyclic aromatic hydrocarbons (PAHs) in the Mediterranean Sea: atmospheric occurrence, deposition and decoupling with settling fluxes in the water column. Environ. Pollut. 166, 40–47. https://doi.org/10.1016/j.envpol.2012.03.003.
Catalá, T.S., Reche, I., Álvarez, M., Khatiwala, S., Guallart, E.F., Benítez-Barrios, V.M., Fuentes-Lema, A., Romera-Castillo, C., Nieto-Cid, M., Pelejero, C., Fraile-Nuez, E., Ortega-Retuerta, E., Marrasé, C., Álvarez-Salgado, X.A., 2015. Water mass age and aging driving chromophoric dissolved organic matter in the dark global ocean. Glob. Biogeochem. Cycles 29 (7), 917–934. https://doi.org/10.1002/2014GB005048.
Catalá, T.S., Álvarez-Salgado, X.A., Otero, J., Iuculano, F., Companys, B., Horstkotte, B., Romera-Castillo, C., Nieto-Cid, M., Latasa, M., Moràn, X.A.G., Gasol, J.M., Marrasé, C., Stedmon, C.A., Reche, I., 2016. Drivers of fluorescent dissolved organic matter in the global epipelagic ocean. Limnol. Oceanogr. 61 (3), 1101–1119. https://doi.org/10.1002/lno.10281.
Catalá, T.S., Marenez–Pérez, A.M., Nieto–Cid, M., Álvarez, M., Otero, J., Emelianov, M., Reche, I., Arístegui, J., Álvarez–Salgado, X.A., 2018. Dissolved Organic Matter (DOM) in the open Mediterranean Sea. I. Basin–wide distribution and drivers of chromophoric DOM. Prog. Oceanogr. 165, 35–51. https://doi.org/10.1016/j.pocean.2018.05.002.
Cawley, K.M., Ding, Y., Fourqurean, J., Jaffé, R., 2012. Characterising the sources and fate of dissolved organic matter in shark Bay, Australia: a preliminary study using optical properties and stable carbon isotopes. Mar. Freshw. Res. 63 (11), 1098–1107. https://doi.org/10.1071/MF12028.
Claustre, H., Morel, A., Hooker, S.B., Babin, M., Antoine, D., Oubelkheir, K., Maritorena, S., 2002. Is desert dust making oligotrophic waters greener? Geophys. Res. Lett. 29 (10), 107–1–107-4. https://doi.org/10.1029/2001GL014056.
Coble, P.G., 1996. Characterization of marine and terrestrial DOM in seawater using excitation-emission matrix spectroscopy. Mar. Chem. 51, 325–346. https://doi.org/10.1016/0304-4203(95)00062-3.
De Stephanis, R., Cornulier, T., Verborgh, P., Sierra, J.S., Gimeno, N.P., Guinet, C., 2008. Summer spatial distribution of cetaceans in the Strait of Gibraltar in relation to the oceanographic context. Mar. Ecol. Prog. Ser. 353, 275–288. https://doi.org/10.3354/meps07164.
De Vicente, I., Ortega-Retuerta, E., Morales-Baquero, R., Reche, I., 2012. Contribution of dust inputs to dissolved organic carbon and water transparency in Mediterranean reservoirs. Biogeosciences 9, 5049–5060. https://doi.org/10.5194/bg-9-5049-2012.
Djaoudi, K., Van Wambeke, F., Barani, A., Hélias-Nunige, S., Sempéré, R., Pulido-Villena, E., 2018. Atmospheric fluxes of soluble organic C, N, and P to the Mediterranean Sea: potential biogeochemical implications in the surface layer. Prog. Oceanogr. 163, 59–69. https://doi.org/10.1016/j.pocean.2017.07.008.
Economou, C., Mihalopoulos, N., 2002. Formaldehyde in the rainwater in the eastern Mediterranean: occurrence, deposition and contribution to organic carbon budget. Atmos. Environ. 36 (8), 1337–1347. https://doi.org/10.1016/S1352-2310(01)00555-6.
Ferretto, N., Tedetti, M., Guigue, C., Mounier, S., Redon, R., Goutx, M., 2014. Identification and quantification of known polycyclic aromatic hydrocarbons and pesticides in complex mixtures using fluorescence excitation–emission matrices and parallel factor analysis. Chemosphere 107, 344–353. https://doi.org/10.1016/j.chemosphere.2013.12.087.
Fichot, C.G., Benner, R., 2012. The spectral slope coefficient of chromophoric dissolved organic matter (S275-295) as a tracer of terrigenous dissolved organic carbon in river-influenced ocean margins. Limnol. Oceanogr. 57, 1453–1466. https://doi.org/10.4319/lo.2012.57.5.1453.
Garcia, H.E., Gordon, L.I., 1992. Oxygen solubility in seawater: better fitting equations. Limnol. Oceanogr. 37 (6), 1307–1312. https://doi.org/10.4319/lo.1992.37.6.1307.
Gonnelli, M., Vestri, S., Santinelli, C., 2013. Chromophoric dissolved organic matter and microbial enzymatic activity. A biophysical approach to understand the marine carbon cycle. Biophys. Chem. https://doi.org/10.1016/j.bpc.2013.06.016.
Gonnelli, M., Galletti, Y., Marchetti, E., Mercadante, L., Brogi, S.R., Ribotti, A., Sorgente, R., Vestri, S., Santinelli, C., 2016. Dissolved organic matter dynamics in surface waters affected by oil spill pollution: results from the Serious Game exercise. Deep Sea Res. Part II: Top. Stud. Oceanogr. 133, 88–99. https://doi.org/10.1016/j.dsr2.2016.05.027.
Granskog, M.A., Nomura, D., Müller, S., Krell, A., Toyota, T., Hattori, H., 2015. Evidence for significant protein-like dissolved organic matter accumulation in Sea of Okhotsk sea ice. Ann. Glaciol. 56 (69), 1–8. https://doi.org/10.3189/2015AoG69A002.
Green, S.A., Blough, N.V., 1994. Optical absorption and fluorescence properties of chromophoric dissolved organic matter in natural waters. Limnol. Oceanogr. 39 (8), 1903–1916. https://doi.org/10.4319/lo.1994.39.8.1903.
Hansell, D.A., 2002. DOC in the global ocean carbon cycle. In: Hansell, D.A., Carlson, C.A. (Eds.), Biogeochemestry of Marine Dissolved Organic Matter, First ed. Academic Press, San Diego, pp. 685–714. https://doi.org/10.1016/B978-012323841-2/50017-8.
Hansell, D.A., 2005. Dissolved organic carbon reference material program. Eos Trans. Am. Geophys. Union 86 (35). https://doi.org/10.1029/2005EO350003. (318-318).
Hansell, D.A., Carlson, C.A., Repeta, D.J., Schiltzer, R., 2009. Dissolved organic matter in the ocean: a controversy stimulates new insights. Oceanography 22 (4), 202–211. https://doi.org/10.5670/oceanog.2009.109.
Hansell, D.A., 2013. Recalcitrant dissolved organic carbon fractions. Annu. Rev. Mar. Sci. 5 (2013), 421–445. https://doi.org/10.1146/annurev-marine-120710-100757.
Hansell, D.A., Carlson, C.A., 2013. Localized refractory dissolved organic carbon sinks in the deep ocean. Glob. Biogeochem. Cycles 27 (3), 705–710. https://doi.org/10.1002/gbc.20067.
Hayase, K., Shinozuka, N., 1995. Vertical distribution of fluorescent organic matter along with AOU and nutrients in the equatorial Central Pacific. Mar. Chem. 48 (3–4), 283–290. https://doi.org/10.1016/0304-4203(94)00051-E.
Helms, J.R., Stubbins, A., Ritchie, J.D., Minor, E.C., Kieber, D.J., Mopper, K., 2008. Absorption spectral slopes and slope ratios as indicators of molecular weight, source, and photobleaching of chromophoric dissolved organic matter. Limnol. Oceanogr. 53 (3), 955–969. https://doi.org/10.4319/lo.2008.53.3.0955.
Jiao, N., Herndl, G.J., Hansell, D.A., Benner, R., Kattner, G., Wilhelm, S.W., Kirchman, D.L., Weinbauer, M.G., Luo, T., Chen, F., Azam, F., 2010. Microbial production of recalcitrant dissolved organic matter: long-term carbon storage in the global ocean. Nat. Rev. Microbiol. 8 (8), 593. https://doi.org/10.1038/nrmicro2386.
Jørgensen, L., Stedmon, C.A., Kragh, T., Markager, S., Middelboe, M., Søndergaard, M., 2011. Global trends in the fluorescence characteristics and distribution of marine dissolved organic matter. Mar. Chem. 126, 139–148. https://doi.org/10.1016/j.marchem.2011.05.002.
Jørgensen, L., Stedmon, C.A., Granskog, M.A., Middelboe, M., 2014. Tracing the long--term microbial production of recalcitrant fluorescent dissolved organic matter in seawater. Geophys. Res. Lett. 41 (7), 2481–2488. https://doi.org/10.1002/2014GL059428.
Kanakidou, M., Duce, R.A., Prospero, J.M., Baker, A.R., Benitez-Nelson, C., Dentener, F.J., Hunter, K.A., Liss, P.S., Mahowald, N., Okin, G.S., Sarin, M., Tsigaridis, K., Uematsu, M., Zamora, L.M., Zhu, T., 2012. Atmospheric fluxes of organic N and P to the global ocean. Glob. Biogeochem. Cycles 26 (3). https://doi.org/10.1029/2011GB004277.
Kowalczuk, P., Durako, M.J., Young, H., Kahn, A.E., Cooper, W.J., Gonsior, M., 2009. Characterization of dissolved organic matter fluorescence in the South Atlantic Bight with use of PARAFAC model: interannual variability. Mar. Chem. 113, 182–196. https://doi.org/10.1016/j.marchem.2009.01.015.
Lacowicz, J.R., 2006. Principles of Fluorescence Spectroscopy. Springer, Baltimore.
Lawaetz, A.J., Stedmon, C.A., 2009. Fluorescence intensity calibration using the Raman scatter peak of water. Appl. Spectrosc. 63 (8), 936–940. https://doi.org/10.1366/000370209788964548.
Lin, H., Guo, W., Hu, M., Lin, C., Ji, W., 2012. Spatial and temporal variability of colored dissolved organic matter absorption properties in the Taiwan Strait. Acta Oceanol. Sin. 31 (5), 98–106. https://doi.org/10.1007/s13131-012-0240-x.
Lønborg, C., Yokokawa, T., Herndl, G.J., Álvarez-Salgado, X.A., 2015. Production and degradation of fluorescent dissolved organic matter in surface waters of the eastern north Atlantic ocean. Deep Sea Res. Part I: Oceanogr. Res. Pap. 96, 28–37. https://doi.org/10.1016/j.dsr.2014.11.001.
Luna, G.M., 2015. Diversity of marine microbes in a changing Mediterranean Sea. Rend. Fis. Acc. Lincei 26, 49–58. https://doi.org/10.1007/s12210-014-0333-x.
Malcolm, R.L., Aiken, G.R., Bowles, E.C., Malcolm, J.D., 1982. Isolation of fulvic and humic acids from the Suwannee River. Humic substances in Suwannee River, Georgia: interactions, properties and proposed structures. U. S. Geol. Surv. Water-Supply Pap. 2373, 13–18.
Maqbool, T., Cho, J., Hur, J., 2017. Spectroscopic descriptors for dynamic changes of soluble microbial products from activated sludge at different biomass growth phases under prolonged starvation. Water Res. 123, 751–760. https://doi.org/10.1016/j.watres.2017.07.033.
Margolin, A.R., Gerringa, L.J., Hansell, D.A., Rijkenberg, M.J., 2016. Net removal of dissolved organic carbon in the anoxic waters of the Black Sea. Mar. Chem. 183, 13–24. https://doi.org/10.1016/j.marchem.2016.05.003.
Margolin, A.R., Gonnelli, M., Hansell, D.A., Santinelli, C., 2018. Black Sea dissolved organic matter dynamics: insights from optical analyses. Limnol. Oceanogr. https://doi.org/10.1002/lno.10791.
Martínez-Pérez, A.M., Osterholz, H., Nieto-Cid, M., Álvarez, M., Dittmar, T., Álvarez-Salgado, X.A., 2017a. Molecular composition of dissolved organic matter in the Mediterranean Sea. Limnol. Oceanogr. 62 (6), 2699–2712. https://doi.org/10.1002/lno.10600.
Martínez-Pérez, A.M., Nieto-Cid, M., Osterholz, H., Catalá, T.S., Reche, I., Dittmar, T., Álvarez-Salgado, X.A., 2017b. Linking optical and molecular signatures of dissolved organic matter in the Mediterranean Sea. Sci. Rep. 7 (1), 3436. https://doi.org/10.1038/s41598-017-03735-4.
Meng, F., Dai, M., Cao, Z., Wu, K., Zhao, X., Li, X., Chen, J., Gan, J., 2017. Seasonal dynamics of dissolved organic carbon under complex circulation schemes on a large continental shelf: the Northern South China Sea. J. Geophys. Res.: Oceans 122 (12), 9415–9428. https://doi.org/10.1002/2017JC013325.
Mopper, K., Schultz, C.A., 1993. Fluorescence as a possible tool for studying the nature and water column distribution of DOC components. Mar. Chem. 41, 229–238. https://doi.org/10.1016/0304-4203(93)90124-7.
Morel, A., Claustre, H., Antoine, D., Gentili, B., 2007. Natural variability of bio-optical properties in Case 1 waters: attenuation and reflectance within the visible and near-UV spectral domains, as observed in South Pacific and Mediterranean waters. Biogeosciences Discuss. 4 (4), 2147–2178.
Morel, A., Gentili, B., 2009. The dissolved yellow substance and the shades of blue in the Mediterranean Sea. Biogeosciences 6 (11), 2625–2636. https://doi.org/10.5194/bg-6-2625-2009.
Murphy, K.R., Ruiz, G.M., Dunsmuir, W.T., Waite, T.D., 2006. Optimized parameters for fluorescence-based verification of ballast water exchange by ships. Environ. Sci. Technol. 40 (7), 2357–2362. https://doi.org/10.1016/j.marchem.2007.10.003.
Murphy, K.R., Stedmon, C.A., Waite, T.D., Ruiz, G.M., 2008. Distinguishing between terrestrial and autochthonous organic matter in marine environments using fluorescence spectroscopy. Mar. Chem. 108, 40–58. https://doi.org/10.1016/j.marchem.2007.10.003.
Murphy, K.R., Hambly, A., Singh, S., Henderson, R.K., Baker, A., Stuetz, R., Khan, S.J., 2011. Organic matter fluorescence in municipal water recycling schemes: toward a unified PARAFAC model. Environ. Sci. Technol. 45 (7), 2909–2916. https://doi.org/

10.1021/es103015e.
Murphy, K.R., Stedmon, C.A., Wenig, P., Bro, R., 2014. OpenFluor – an online spectral library of auto-fluorescence by organic compounds in the environment. Anal. Methods 6 (3), 658–661. https://doi.org/10.1039/C3AY41935E.
Nakatsuka, T., Toda, M., Kawamura, K., Wakatsuchi, M., 2004. Dissolved and particulate organic carbon in the Sea of Okhotsk: transport from continental shelf to ocean interior. J. Geophys. Res.: Oceans 109 (C9). https://doi.org/10.1029/2003JC001909.
Nelson, N.B., Carlson, C.A., Steinberg, D.K., 2004. Production of chromophoric dissolved organic matter by Sargasso Sea microbes. Mar. Chem. 89 (1–4), 273–287. https://doi.org/10.1016/j.marchem.2004.02.017.
Nelson, N.B., Siegel, D.A., Carlson, C.A., Swan, C., Smethie Jr, W.M., Khatiwala, S., 2007. Hydrography of chromophoric dissolved organic matter in the North Atlantic. Deep-Sea Reas. I 54, 710–731. https://doi.org/10.1016/j.dsr.2007.02.006.
Nelson, N.B., Siegel, D.A., Carlson, C.A., Swan, C.M., 2010. Tracing global biogeochemical cycles and meridional overturning circulation using chromophoric dissolved organic matter. Geophys. Res. Lett. 37 (3). https://doi.org/10.1029/2009GL042325.
Nelson, N.B., Siegel, D.A., 2013. The global distribution and dynamics of chromophoric dissolved organic matter. Annu. Rev. Mar. Sci. 5, 447–476. https://doi.org/10.1146/annurev-marine-120710-100751.
Nelson, N.B., Gauglitz, J.M., 2016. Optical signatures of dissolved organic matter transformation in the global ocean. Front. Mar. Sci. 2, 118. https://doi.org/10.3389/fmars.2015.00118.
Nieto-Cid, M., Álvarez-Salgado, X.A., Gago, J., Pérez, F.F., 2005. DOM fluorescence, a tracer for biogeochemical processes in a coastal upwelling system (NW Iberian Peninsula). Mar. Ecol. Prog. Ser. 297, 33–50. https://doi.org/10.3354/meps297033.
Organelli, E., Bricaud, A., Antoine, D., Matsuoka, A., 2014. Seasonal dynamics of light absorption by chromophoric dissolved organic matter (CDOM) in the NW Mediterranean Sea (BOUSSOLE site). Deep Sea Res. Part I: Oceanogr. Res. Pap. 91, 72–85. https://doi.org/10.1016/j.dsr.2014.05.003.
Organelli, E., Claustre, H., Bricaud, A., Barbieux, M., Uitz, J., D'Ortenzio, F., Dall'Olmo, G., 2017. Bio-optical anomalies in the world's oceans: an investigation on the diffuse attenuation coefficients for downward irradiance derived from Biogeochemical Argo float measurements. J. Geophys. Res.: Oceans 122 (5), 3543–3564. https://doi.org/10.1002/2016JC012629.
Osburn, C.L., Stedmon, C.A., 2011. Linking the chemical and optical properties of dissolved organic matter in the Baltic–North Sea transition zone to differentiate three allochthonous inputs. Mar. Chem. 126 (1–4), 281–294. https://doi.org/10.1016/j.marchem.2011.06.007.
Painter, S.C., Lapworth, D.J., Woodward, E.M.S., Kroeger, S., Evans, C.D., Mayor, D.J., Sanders, R.J., 2018. Terrestrial dissolved organic matter distribution in the North Sea. Sci. Total Environ. 630, 630–647. https://doi.org/10.1016/j.scitotenv.2018.02.237.
Para, J., Coble, P.G., Charrière, B., Tedetti, M., Fontana, C., Sempéré, R., 2010. Fluorescence and absorption properties of chromophoric dissolved organic matter (CDOM) in coastal surface waters of the northwestern Mediterranean Sea, influence of the Rhône River. Biogeosciences 7 (12), 4083–4103. https://doi.org/10.5194/bg-7-4083-2010.
Pérez, G.L., Galí, M., Royer, S.J., Sarmento, H., Gasol, J.M., Marrasé, C., Simó, R., 2016. Bio-optical characterization of offshore NW Mediterranean waters: cdom contribution to the absorption budget and diffuse attenuation of downwelling irradiance. Deep Sea Res. Part I: Oceanogr. Res. Pap. 114, 111–127. https://doi.org/10.1016/j.dsr.2016.05.011.
Pitta, E., Zeri, C., Tzortziou, M., Mousdis, G., Scoullos, M., 2017. Seasonal variations in dissolved organic matter composition using absorbance and fluorescence spectroscopy in the Dardanelles Straits–North Aegean Sea mixing zone. Cont. Shelf Res. 149, 82–95. https://doi.org/10.1016/j.csr.2016.07.013.
Pulido-Villena, E., Wagener, T., Guieu, C., 2008. Bacterial response to dust pulses in the western Mediterranean: implications for carbon cycling in the oligotrophic ocean. Glob. Biogeochem. Cycles 22 (1). https://doi.org/10.1029/2007GB003091.
Retelletti Brogi, S., Gonnelli, M., Vestri, S., Santinelli, C., 2015. Biophysical processes affecting DOM dynamics at the Arno river mouth (Tyrrhenian Sea). Biophys. Chem. 197, 1–9. https://doi.org/10.1016/j.bpc.2014.10.004.
Ribera d'Alcalà, M., Civitarese, G., Conversano, F., Lavezza, R., 2003. Nutrient ratios and fluxes hint at overlooked processes in the Mediterranean Sea. J. Geophys. Res.: Oceans 108 (C9). https://doi.org/10.1029/2002JC001650.
Romera-Castillo, C., Sarmento, H., Alvarez-Salgado, X.A., Gasol, J.M., Marraséa, C., 2010. Production of chromophoric dissolved organic matter by marine phytoplankton. Limnol. Oceanogr. 55 (1), 446–454. https://doi.org/10.4319/lo.2010.55.1.0446.
Romera-Castillo, C., Sarmento, H., Álvarez-Salgado, X.A., Gasol, J.M., Marrasé, C., 2011. Net production/consumption of fluorescent coloured dissolved organic matter by natural bacterial assemblages growing on marine phytoplankton exudates. Appl. Environ. Microbiol. 00200. https://doi.org/10.1128/AEM.00200-11.
Rowe, O.F., Dinasquet, J., Paczkowska, J., Figueroa, D., Riemann, L., Andersson, A., 2018. Major differences in dissolved organic matter characteristics and bacterial processing over an extensive brackish water gradient, the Baltic Sea. Mar. Chem. 202, 27–36. https://doi.org/10.1016/j.marchem.2018.01.010.
Sánchez-Pérez, E.D., Marín, I., Nunes, S., Fernández-González, L., Peters, F., Pujo-Pay, M., Conan, P., Marrasé, C., 2016. Aerosol inputs affect the optical signatures of dissolved organic matter in NW Mediterranean coastal waters. Sci. Mar. 80 (4), 437–446. https://doi.org/10.3989/scimar.04318.20B.
Santinelli, C., Ribotti, A., Sorgente, R., Gasparini, G.P., Nannicini, L., Vignudelli, S., Seritti, A., 2008. Coastal dynamics and dissolved organic carbon in the western Sardinian shelf (Western Mediterranean). J. Mar. Syst. 74 (1–2), 167–188. https://doi.org/10.1016/j.jmarsys.2007.12.005.
Santinelli, C., Nannicini, L., Seritti, A., 2010. DOC dynamics in the meso and bathypelagic layers of the Mediterranean Sea. Deep Sea Res. II 57, 1446–1459. https://doi.org/10.1016/j.dsr2.2010.02.014.
Santinelli, C., Hansell, D.A., d'Alcalà, M.R., 2013. Influence of stratification on marine dissolved organic carbon (DOC) dynamics: the Mediterranean Sea case. Progress. Oceanogr. 119, 68–77. https://doi.org/10.1016/j.pocean.2013.06.001.
Santinelli, 2015a. DOC in the Mediterranean Sea. In: Hansell, D.A., Carlson, C.A. (Eds.), Biogeochemestry of Marine Dissolved Organic Matter, Second ed. Academic Press, San Diego, pp. 579–608. https://doi.org/10.1016/B978-0-12-405940-5.00013-3.
Santinelli, C., Follett, C., Brogi, S.R., Xu, L., Repeta, D., 2015b. Carbon isotope measurements reveal unexpected cycling of dissolved organic matter in the deep Mediterranean Sea. Mar. Chem. 177, 267–277. https://doi.org/10.1016/j.marchem.2015.06.018.
Senesi, N., Miano, T.M., Provenzano, M.R., Brunetti, G., 1989. Spectroscopic and compositional comparative characterization of IHSS reference and standard fulvic and humic acids of various origin. Sci. Total Environ. 81, 143–156. https://doi.org/10.1016/0048-9697(89)90120-4.
Seritti, A., Russo, D., Nannicini, L., Del Vecchio, R., 1998. DOC, absorption and fluorescence properties of estuarine and coastal waters of the northern Tyrrhenian Sea. Chem. Speciat. Bioavailab. 10 (3), 95–106. https://doi.org/10.3184/095422998782775790.
Siegel, D.A., Maritorena, S., Nelson, N.B., Hansell, D.A., Kayser-Lorenzi, M., 2002. Global distributions and dynamics of colored dissolved and detrital organic materials. J. Geophys. Res. 107 (C12), 3228. https://doi.org/10.1029/2001JC000965.
Speicher, E.A., Moran, S.B., Burd, A.B., Delfanti, R., Kaberi, H., Kelly, R.P., Papucci, C., Smith, J.N., Stavrakakis, S., Torricelli, L., Zervakis, V., 2006. Particulate organic carbon export fluxes and size-fractionated POC/234Th ratios in the Ligurian, Tyrrhenian and Aegean Seas. Deep Sea Res. Part I: Oceanogr. Res. Pap. 53 (11), 1810–1830. https://doi.org/10.1016/j.dsr.2006.08.005.
Stedmon, C.A., Markager, S., Bro, R., 2003. Tracing dissolved organic matter in aquatic environments using a new approach to fluorescence spectroscopy. Mar. Chem. 82 (3–4), 239–254. https://doi.org/10.1016/S0304-4203(03)00072-0.
Stedmon, C.A., Markager, S., 2005a. Resolving the variability in dissolved organic matter fluorescence in a temperate estuary and its catchment using PARAFAC analysis. Limnol. Oceanogr. 50, 686–697. https://doi.org/10.4319/lo.2005.50.2.0686.
Stedmon, C.A., Markager, S., 2005b. Tracing the production and degradation of autochthonous fractions of dissolved organic matter by fluorescence analysis. Limnol. Oceanogr. 50, 1415–1426. https://doi.org/10.4319/lo.2005.50.5.1415.
Stedmon, C.A., Markager, S., Tranvik, L., Kronberg, L., Slätis, T., Martinsen, W., 2007. Photochemical production of ammonium and transformation of dissolved organic matter in the Baltic Sea. Mar. Chem. 104 (3), 227–240. https://doi.org/10.1016/j.marchem.2006.11.005.
Stedmon, C.A., Bro, R., 2008. Characterizing dissolved organic matter fluorescence with parallel factor analysis: a tutorial. Limnol. Oceanogr.: Methods 6 (11), 572–579. https://doi.org/10.4319/lom.2008.6.572.
Vignudelli, S., Santinelli, C., Murru, E., Nannicini, L., Seritti, A., 2004. Distributions of dissolved organic carbon (DOC) and chromophoric dissolved organic matter (CDOM) in coastal waters of the northern Tyrrhenian Sea (Italy). Estuar. Coast. Shelf Sci. 60 (1), 133–149. https://doi.org/10.1016/j.ecss.2003.11.023.
Vodacek, A., Blough, N.V., DeGrandpre, M.D., Peltzer, E.T., Nelson, R.K., 1997. Seasonal variation of CDOM and DOC in the Middle Atlantic Bight: terrestrial inputs and photooxidation. Limnol. Oceanogr. 42, 674–686. https://doi.org/10.4319/lo.1997.42.4.0674.
Walker, S.A., Amon, R.M., Stedmon, C., Duan, S., Louchouarn, P., 2009. The use of PARAFAC modeling to trace terrestrial dissolved organic matter and fingerprint water masses in coastal Canadian Arctic surface waters. J. Geophys. Res. 114 (G4). https://doi.org/10.1029/2009JG000990.
Wang, C., Guo, W., Li, Y., Stubbins, A., Li, Y., Song, G., Wang, L., Cheng, Y., 2017. Hydrological and biogeochemical controls on absorption and fluorescence of dissolved organic matter in the Northern South China Sea. J. Geophys. Res.: Biogeosciences 122 (12), 3405–3418. https://doi.org/10.1002/2017JG004100.
Weishaar, J.L., Aiken, G.R., Bergamaschi, B.A., Fram, M.S., Fujii, R., Mopper, K., 2003. Evaluation of specific ultraviolet absorbance as an indicator of the chemical composition and reactivity of dissolved organic carbon. Environ. Sci. Technol. 37 (20), 4702–4708. https://doi.org/10.1021/es030360x.
Willey, J.D., Kieber, R.J., Eyman, M.S., Avery, G.B., 2000. Rainwater dissolved organic carbon: concentrations and global flux. Glob. Biogeochem. Cycles 14 (1), 139–148. https://doi.org/10.1029/1999GB900036.
Williams, P.JleB., Jenkinson, N.W., 1982. A transportable microprocessor-controlled Precise Winkler titration suitable for field station and shipboard use. Limnol. Oceanogr. 27 (3), 576–584. https://doi.org/10.4319/lo.1982.27.3.0576.
Yamashita, Y., Tsukasaki, A., Nishida, T., Tanoue, E., 2007. Vertical and horizontal distribution of fluorescent dissolved organic matter in the Southern Ocean. Mar. Chem. 106 (3–4), 498–509. https://doi.org/10.1016/j.marchem.2007.05.004.
Yamashita, Y., Tanoue, E., 2008. Production of bio-refractory fluorescent dissolved organic matter in the ocean interior. Nat. Geosci. 1 (9), 579.
Yamashita, Y., Jaffé, R., Maie, N., Tanoue, E., 2008. Assessing the dynamics of dissolved organic matter (DOM) in coastal environments by excitation emission matrix fluorescence and parallel factor analysis (EEM-PARAFAC). Limnol. Oceanogr. 53 (5), 1900–1908. https://doi.org/10.4319/lo.2008.53.5.1900.
Yamashita, Y., Tanoue, E., 2009. Basin scale distribution of chromophoric dissolved organic matter in the Pacific Ocean. Limnol. Oceanogr. 54 (2), 598–609. https://doi.org/10.4319/lo.2009.54.2.0598.
Yamashita, Y., Scinto, L.J., Maie, N., Jaffé, R., 2010a. Dissolved organic matter characteristics across a subtropical wetland's landscape: application of optical properties in the assessment of environmental dynamics. Ecosystems 13 (7), 1006–1019. https://doi.org/10.1007/s10021-010-9370-1.
Yamashita, Y., Cory, R.M., Nishioka, J., Kuma, Tanoue E., Jaffé, R., 2010b. Fluorescence

characteristics of dissolved waters of the Okhotsk Sea and northwestern North Pacific Ocean. Deep-sea Res. II 57, 1478–1485. https://doi.org/10.1016/j.dsr2.2010.02.016.
Yamashita, Y., Boyer, J.N., Jaffé, R., 2013. Evaluating the distribution of terrestrial dissolved organic matter in a complex coastal ecosystem using fluorescence spectroscopy. Cont. Shelf Res. 66, 136–144. https://doi.org/10.1016/j.csr.2013.06.010.
Xing, X., Claustre, H., Wang, H., Poteau, A., D'Ortenzio, F., 2014. Seasonal dynamics in colored dissolved organic matter in the Mediterranean Sea: patterns and drivers. Deep-Sea Res. Part I: Oceanogr. Res. Pap. 93–101. https://doi.org/10.1016/j.dsr.2013.09.008.
Zhao, Y., Song, K., Shang, Y., Shao, T., Wen, Z., Lv, L., 2017. Characterization of CDOM of river waters in China using fluorescence excitation-emission matrix and regional integration techniques. J. Geophys. Res.: Biogeosci. 122 (8), 1940–1953. https://doi.org/10.1002/2017JG003820.
Zhou, F., Gao, X., Song, J., Chen, C.T.A., Yuan, H., Xing, Q., 2018. Absorption properties of chromophoric dissolved organic matter (CDOM) in the East China Sea and the waters off eastern Taiwan. Cont. Shelf Res. 159, 12–23. https://doi.org/10.1016/j.csr.2018.03.005.
Zhu, W.Z., Zhang, H.H., Zhang, J., Yang, G.P., 2018. Seasonal variation in chromophoric dissolved organic matter and relationships among fluorescent components, absorption coefficients and dissolved organic carbon in the Bohai Sea, the Yellow Sea and the East China Sea. J. Mar. Syst. 180, 9–23. https://doi.org/10.1016/j.jmarsys.2017.12.003.